

# Bayesian mortality modelling with pandemics: a vanishing jump approach

Julius Goes <sup>\*1</sup>, Karim Barigou <sup>†2</sup>, and Anne Leucht <sup>‡1</sup>

<sup>1</sup>*University of Bamberg, Institute of Statistics, Bamberg, Germany*

<sup>2</sup>*Ecole d'actuariat, Université Laval, 2425, rue de l'Agriculture, Québec (GQ) G1V 0A6, Canada*

Version: November 10, 2023

## Abstract

This paper extends the Lee-Carter model to include vanishing jumps on mortality rates, where the impact is highest in the beginning and then gradually diminishes. Existing models either account for transitory jumps over one period or permanent shifts. However, there is no literature on estimating mortality time series with jumps that have a vanishing effect over a small number of periods, as is typically observed in pandemics. Using COVID-19 data, our proposed Bayesian model outperforms transitory shock models in terms of in-sample fit, thus providing a more comprehensive representation of mortality rates during a pandemic.

**Keywords:** Stochastic mortality modelling, Pandemic shocks, jump effects, Bayesian inference.

## 1 Introduction

The model of [Lee and Carter \(1992\)](#) has been widely used in actuarial science and demography to forecast mortality rates based on past observations. This model assumes that mortality rates follow a stochastic trend with a time-dependent mortality factor, adjusted for age-specific effects, using two sets of age-dependent coefficients. While this model has shown to be effective in capturing mortality trends in many countries, it may not be able to adequately account for large, unexpected jumps in mortality rates, such as those caused by pandemics ([Chen et al., 2022](#), [van Berkum et al., 2022](#)). In this paper, we extend the Lee-Carter model and introduce a framework that is suitable in capturing the typical effects of a pandemic on the subsequent age-specific mortality rates. That is, we introduce a model that integrates vanishing shocks, where the shock's impact is highest in the beginning and then gradually diminishes in the subsequent years.

The COVID-19 pandemic has emphasised the importance of incorporating mortality shocks into the Lee-Carter (LC) model. While jump effects have been introduced in previous studies, they often fail to account for age-specific pandemic effects. [Cox et al. \(2006\)](#) and [Chen and Cox \(2009\)](#) proposed

---

<sup>\*</sup>julius.goes@uni-bamberg.de

<sup>†</sup>karim.barigou@act.ulaval.ca

<sup>‡</sup>anne.leucht@uni-bamberg.de

extensions with permanent and transitory jump effects, respectively, but the jump effect is applied to the time-dependent factor instead of the mortality rates. This means, that the age pattern of a potential shock is identical to that of the general mortality improvement. To address this shortcoming, [Liu and Li \(2015\)](#) extended the Lee-Carter model by including a time- and age-dependent jump effect, which allows, for example, to capture the age-specific effect of COVID-19. However, their method only allows the inclusion of transitory mortality shocks that last one period, i.e. one year. Here, these effects are incorporated using independent and identically distributed (i.i.d.) shock variables. Consequently, during years of pandemic, mortality rates experience an upward shift. However, this model has a limitation in its assumption of a time-independent jump variable. Specifically, it implies that during years with consecutive shocks, the severity of mortality rate adjustments is independent, or for years following a single-period shock, the effect completely vanishes in the subsequent year. Such assumptions are inconsistent with observed pandemic patterns, wherein mortality rates are heavily impacted during initial stages and gradually taper off.

In the aftermath of the COVID pandemic, a variety of models were proposed to capture the nuances of mortality trends. For example, [van Berkum et al. \(2022\)](#) extended the multi-population model originally proposed by [Li and Lee \(2005\)](#) for this purpose. Their model integrates three layers: the first two focusing on pre-COVID mortality trends and the third specifically capturing the excess mortality attributable to COVID. The framework offers mortality forecasts based on a spectrum of potential pandemic trajectories, determined by a parameter which varies between 0 and 1, yet remains uncalibrated. Meanwhile, [Zhou and Li \(2022\)](#) introduced a tri-level model to simulate future mortality scenarios influenced by events similar to the COVID outbreak. The intricacies of the pandemic's progression are encapsulated within their model's third layer, which is heavily informed by expert insights. Further broadening the scope, [Chen et al. \(2022\)](#) developed a multi-country mortality framework which incorporates two distinct jump components: one signifying global pandemic shocks, and the other reflecting country-specific disturbances. [Robben and Antonio \(2023\)](#) applied a multi-population regime switching model to switch between periods of high volatility states (i.e. shock years) and low volatility states. However, they also assume uncorrelated one period shocks. [Richards \(2023\)](#) on the other hand discusses techniques for robust estimation of mortality rates in the presence of outliers, with a scenario included for gradually diminishing effects.

All the previous literature that tries to account for vanishing jumps is using either expert opinions or simulation studies based on possible vanishing scenarios. Moreover, the estimation procedure is based on a frequentist multi-step process. To better reflect this dynamic nature of a pandemic, we integrate the vanishing jump component in our single-step model estimation procedure, which allows to estimate the vanishing effect and its uncertainty in a consistent and data-driven way. Hereby, we adopt a Bayesian framework for mortality modelling, a decision driven by the inherent advantages of this approach. Specifically, the Bayesian methodology integrates the estimation and forecasting processes, ensuring more consistent and robust estimates as underscored by [Cairns et al. \(2011\)](#) and [Wong et al. \(2018\)](#). Furthermore, this approach excels in accommodating various sources of uncertainty in a coherent manner.

Delving into the historical context, [Czado et al. \(2005\)](#) pioneered the application of a comprehensive Bayesian approach specific to the Poisson Lee-Carter (LC) model. This methodology was later expanded to a multi-population context by [Antonio et al. \(2015\)](#). Other notable contributions include [Pedroza \(2006\)](#), who employed a Bayesian state-space model using Kalman filters to address missing data issues in mortality forecasting. Additionally, [Venter and Şahn \(2018\)](#) leveraged Bayesian shrinkage to achieve a more parsimonious parameterisation for mortality models. The development and wider availability of Markov chain Monte Carlo (MCMC) techniques have further increased the application of Bayesian methodologies in mortality modelling, as evidenced by the growing body of recent work including (e.g. [Alexopoulos et al., 2019](#), [Li et al., 2019](#), [Barigou et al., 2023](#), [Wong et al., 2023](#)).

The remainder of this paper is organised as follows. Section 2 provides the specification of our model, which is composed of a baseline Lee-Carter model and a vanishing jump component with age-specific effect. Section 3 explains how the parameters are estimated. Section 5 presents the estimation results for COVID data from Italy, Spain and United States, and war data from England and Wales. In particular, we compare the performance of our model to the original Lee-Carter model and to the model of Liu and Li (2015) which does not include gradually vanishing effects. Section 6 discusses the projection of future mortality scenarios and Section 7 provides concluding remarks.

## 2 Model specification

Our proposed mortality model builds upon previous work on the Lee-Carter model and its extension with short-term jump effects by Liu and Li (2015). Our model can be seen as a generalisation of their approach, allowing for more flexibility and accuracy in capturing pandemic effects on mortality rates. In this section, we start with a brief overview of both the Lee-Carter model and the Liu-Li model to establish the foundation for our proposed model.

When studying human mortality, the data at hand consist of death counts  $D_{x,t}$  and central exposures  $E_{x,t}$ , where  $x \in \{1, 2, \dots, A\}$  and  $t \in \{1, 2, \dots, T\}$  represent a set of  $A$  age groups and  $T$  calendar years, respectively. We denote by  $m_{x,t}$  the central death rate at age  $x$  and calendar year  $t$  given by

$$m_{x,t} = \frac{D_{x,t}}{E_{x,t}}.$$

### 2.1 The Lee-Carter model

The Lee-Carter model (Lee and Carter, 1992) is a well-known method for modelling mortality rates over time. It assumes that the logarithm of the central death rate  $m_{x,t}$  for age group  $x$  in year  $t$  can be expressed as:

$$\ln(m_{x,t}) = \alpha_x + \beta_x \kappa_t + e_{x,t},$$

where  $\alpha_x$  represents the static level of mortality for age group  $x$ ,  $\kappa_t$  captures the variation of log mortality rates over time,  $\beta_x$  measures the sensitivity of  $\ln(m_{x,t})$  to changes in  $\kappa_t$ , and  $e_{x,t} \stackrel{\text{i.i.d.}}{\sim} \mathcal{N}(0, \sigma_e^2)$  is the error term. In the Lee-Carter model,  $\alpha_x$  and  $\beta_x$  represent age-specific effects, while  $\kappa_t$  is a time-varying factor that captures the overall trend in mortality rates over time. Regarding the estimation, the frequentist approach is usually performed in two steps. First, parameters are obtained by maximising the model log-likelihood, then in a second step, projections are made by time-series techniques (Pitacco, 2009). In a Bayesian approach, the estimation and forecasting steps are performed in a single step, ensuring more consistent estimates in the estimation procedure (Cairns et al., 2011).

Despite its success in modelling mortality rates over time, the Lee-Carter model has a severe limitation when it comes to pandemics as the model assumes that mortality rates evolve smoothly over time, without sudden changes or shocks, driven by a simple random walk with drift.

### 2.2 The Liu-Li model

To introduce short-term jump effects, Liu and Li (2015) proposed an extension of the original Lee-Carter model, which includes an extra jump term as follows:

$$\ln(m_{x,t}) = \alpha_x + \beta_x \kappa_t + N_t J_{x,t} + e_{x,t},$$

Here,  $\alpha_x$ ,  $\beta_x$  and  $e_{x,t}$  have the same meanings as in the original Lee-Carter model, while  $\kappa_t$  is assumed to be a random walk with drift. Additionally,  $N_t$  represents a binary random variable that equals one if a mortality jump occurs in year  $t$  and zero otherwise. The authors assume that the  $N_t$ 's are i.i.d. Bernoulli distributed with parameter  $p$ , denoting the probability of a mortality jump in a calendar year.  $J_{x,t}$  measures the effect of a mortality jump that occurred in year  $t$  on age group  $x$ .

Three specific model variants were proposed, denoted as models J0-J1-J2. Model J1 is the closest to our model and is given by

$$\ln(m_{x,t}) = \alpha_x + \beta_x \kappa_t + \beta_x^{(J)} N_t Y_t + e_{x,t}, \quad (2.1)$$

where  $Y_t$  denotes the effect or severity of the mortality jump at time  $t$ . These jump effects are assumed to be i.i.d. Gaussian variables. Compared to the Lee-Carter model, a new age pattern of pandemic effects  $\beta_x^{(J)}$  is introduced. It is multiplied by the pandemic jump effect to capture age-specific variation, that is different from the period effects  $\beta_x$ .

The model proposed by Liu and Li provides a valuable extension of the Lee-Carter model as it allows the inclusion of short jumps and different age patterns. However, it has two weaknesses: first, this model assumes that age patterns of different mortality shocks are the same, while historically, different age patterns have been observed. For example, half of the deaths caused by the 1918 flu pandemic occurred among 20- to 40-year-olds (Gagnon et al., 2013), while COVID-19 has affected mostly the most vulnerable people (Ferguson et al., 2020, O'Driscoll et al., 2021). In a Bayesian setting however, the pandemic effects  $\beta_x^{(J)}$  are not considered to be fixed. The use of different priors provides a wide range of estimation possibilities. Second, the yearly jumps are independent and the Liu-Li model does not allow for a jump event lasting over several years with a vanishing effect as it can be observed for COVID-19. Our model presented in the next section allows for such an extension.

### 2.3 Our model with gradually vanishing jump effects

The limitations of the Lee-Carter model and its extension by Liu and Li (2015) motivate the need for a more flexible model that can capture the influence of a pandemic lasting over several years with a vanishing effect. Several recent studies have addressed this issue by proposing extensions to the Lee-Carter model. For instance, van Berkum et al. (2022) and Zhou and Li (2022) discussed the idea of a vanishing effect in the context of COVID-19, but did not try to estimate a corresponding parameter. To address this, we propose a model that allows for pandemic shocks that are transitory and vanishing over time. Our model, formulated in (2.2), extends the Lee-Carter model by adding a pandemic shock component,  $J_t$ , with a vanishing effect at a rate controlled by the parameter  $a \in [0, 1)$ :

$$\begin{aligned} \ln(m_{x,t}) &= \alpha_x + \beta_x \kappa_t + \beta_x^{(J)} J_t + e_{x,t} \\ J_t &= a J_{t-1} + N_t Y_t. \end{aligned} \quad (2.2)$$

Similar to Liu and Li (2015), we model the time effect using a random walk representation

$$\kappa_t = \kappa_{t-1} + d + \xi_t, \quad (2.3)$$

where  $d \neq 0$  denotes the drift parameter and  $(\xi_t)_t$  is a sequence of error terms. The parameter  $Y_t$  denotes the magnitude of the jump effect, and  $N_t \in \{0, 1\}$  indicates the jump occurrences. It should be noted, that in the model of Liu and Li (2015), all of  $Y_t$ ,  $N_t$  and  $\kappa_t$  are defined as random variables, while in our Bayesian formulation, they are treated as parameters with appropriate prior distributions.

The model includes several key components: the age-specific baseline mortality rate  $\alpha_x$ , the period effect  $\beta_x \kappa_t$ , and the jump effect  $\beta_x^{(J)} J_t$ . The state-space structure of the model allows for the inclusion of a time-varying parameter  $\kappa_t$ , that captures the overall trend in mortality rates, and a jump count variable  $N_t$ , that determines whether a jump occurs in year  $t$ . The jump size effect  $J_t$ , captures the impact of the pandemic shock on mortality rates, with the vanishing effect controlled by the parameter  $a \in [0, 1)$ .

Our model (2.2) is a (Bayesian) generalisation of the model J1 in Equation (2.1) of Liu and Li (2015), that is recovered when  $a = 0$  and allows for a gradually vanishing effect when  $a > 0$ . Indeed, if there is a mortality jump in year  $t$ , the impact on the log mortality rates is given by  $\beta_x^{(J)} Y_t$  in year  $t$ , by  $a \beta_x^{(J)} Y_t$  in year  $t + 1$ , and so on. The Bayesian framework we use for parameter estimation provides a full predictive distribution for all parameters, including  $\beta_x^{(J)}$ . Furthermore, the Bayesian setting also enables us to account for the uncertainty of all parameters, including the gradually vanishing effect  $a$  of our model (2.2). This flexibility allows us, for example, to accommodate different age patterns for different mortality jumps, that is for each future shock, we obtain (slightly) different realisations of the age patterns.

### 3 Estimation procedure

For the estimation of mortality models, there are two common routes: either estimate the model on the central death rates directly (the traditional approach), or estimate the model on the first differences of the log mortality rates, also called mortality improvements. These two routes are referred to as *Route I* and *Route II* in the terminology of Haberman and Renshaw (2012). The latter has gained attention in recent years (e.g. Hunt and Villegas, 2023). In this paper, we proceed to Route II as well. Mitchell et al. (2013) conducted an extensive study comparing the Route I and Route II approach of multiple models in terms of in-sample fit, including the LC model as well as variants thereof, and found the Route II method to be superior. Additionally, it has the advantage of eliminating the static age effect  $\alpha_x$  of the model, thereby reducing the number of identifiability constraints needed (see Hunt and Blake (2020) and the next Section 3.1).

In the Route II approach, the mortality improvements are modelled directly, defined as

$$Z_{x,t} := \ln(m_{x,t+1}) - \ln(m_{x,t}). \quad (3.1)$$

Positive values of mortality improvement rates indicate worsening mortality conditions relative to the previous year, while negative mortality improvement rates display an improvement in mortality. Our model specification in (2.2) can then be written as

$$Z_{x,t} = \beta_x (\kappa_{t+1} - \kappa_t) + \beta_x^{(J)} (J_{t+1} - J_t) + \varepsilon_{x,t},$$

where  $\varepsilon_{x,t} = e_{x,t+1} - e_{x,t}$ . It follows, that  $\varepsilon_{x,t} \stackrel{\text{i.i.d.}}{\sim} \mathcal{N}(0, \sigma_r^2)$  with  $\sigma_r^2 = 2\sigma_e^2$ . Using (2.3), this can be restated as

$$\begin{aligned} Z_{x,t} &= \beta_x \Delta \kappa_{t+1} + \beta_x^{(J)} \Delta J_{t+1} + \varepsilon_{x,t} \\ &= \beta_x (d + \xi_{t+1}) + \beta_x^{(J)} \Delta J_{t+1} + \varepsilon_{x,t}. \end{aligned} \quad (3.2)$$

#### 3.1 Identifiability constraints

Several mortality models, including the LC model, suffer from non-identifiability issues, meaning that different sets of parameters result in equivalent likelihoods and consequently the same fitted rates. In

their paper, [Hunt and Blake \(2020\)](#) discuss the problem of non-identifiability in LC type models with multiple age or period functions at length and provide a general theorem for the selection of suitable constraints. Since our proposed model can be seen as an extension thereof, their logic can be applied to find the number of needed constraints.

In a standard LC model, the age effect may be scaled and the time effect shifted to produce a new set of parameters resulting in the same fitted mortality rates. Thus, the parameters are not uniquely determined and can be transformed in two ways, namely

$$\{\tilde{\alpha}_x, \tilde{\beta}_x, \tilde{\kappa}_t\} = \left\{ \alpha_x, \frac{1}{a} \beta_x, a \kappa_t \right\}, \quad (3.3)$$

$$\{\tilde{\alpha}_x, \tilde{\beta}_x, \tilde{\kappa}_t\} = \{\alpha_x - b \beta_x, \beta_x, \kappa_t + b\}, \quad (3.4)$$

for all  $x \in \{1, 2, \dots, A\}$  and  $t \in \{1, 2, \dots, T\}$ .

In principle, the same problem holds for our model formulation as well. Using matrix notation we can rewrite the first equation of (2.2) in a compact way. Let  $\mathbf{B}_x = (\beta_x, \beta_x^{(J)})^\top$  and  $\mathbf{K}_t = (\kappa_t, J_t)^\top$ , then

$$\ln(m_{x,t}) = \alpha_x + \mathbf{B}_x^\top \mathbf{K}_t + e_{x,t}. \quad (3.5)$$

The model in (3.5) has the same structure as the classical LC model and can be thought of a multivariate extension, coined LC2 in the terminology of [Hunt and Blake \(2020\)](#). Unsurprisingly, the model in (3.5) suffers from non-identifiability. Let there be a matrix  $\mathbf{A} \in \mathbb{R}^{2 \times 2}$  that is invertible and a matrix  $\mathbf{D} \in \mathbb{R}^{2 \times 1}$ . Then, according to [Hunt and Blake \(2020, Theorem 1\)](#) equations (3.3) and (3.4) can be generalised to higher dimensions where the parameters of (3.5) can be transformed using

$$\{\tilde{\alpha}, \tilde{\mathbf{B}}_x, \tilde{\mathbf{K}}_t\} = \{\alpha_x, \mathbf{A}^{-1} \mathbf{B}_x, \mathbf{A} \mathbf{K}_t\} \quad (3.6)$$

$$\{\tilde{\alpha}, \tilde{\mathbf{B}}_x, \tilde{\mathbf{K}}_t\} = \{\alpha_x - \mathbf{D}^\top \mathbf{B}_x, \mathbf{B}_x, \mathbf{K}_t + \mathbf{D}\}. \quad (3.7)$$

Since matrix  $\mathbf{A}$  is  $(2 \times 2)$  and  $\mathbf{D}$  is  $(2 \times 1)$ , there are in total six free parameters meaning that we have to impose six identifiability constraints for the model in (3.5).

However, note that Equation (3.5) includes an age specific intercept. When differencing the log mortality rates to obtain  $Z_{x,t}$ , i.e. applying the Route II estimation method, the age specific intercept cancels. In this case, we obtain that  $\mathbf{D} = \mathbf{0}_{2 \times 1}$  in (3.7) and no further identifiability issues arise from (3.7). Consequently, there is a reduced set of identifiability constraints, namely the four entries of the matrix  $\mathbf{A}$ , as only transformations of (3.6) are relevant ([Hunt and Blake, 2020, Appendix A.](#)). Hence, by applying the Route II estimation approach we can reduce the amount of identifiability constraints needed from six to four, by cancelling out the static age function  $\alpha_x$  due to differentiation of the death rates.

As we prove in the Appendix, identification is ensured by imposing the standard sum-to-one constraints on age parameters, that is

$$\sum_{x=1}^A \beta_x = 1 \quad \text{and} \quad \sum_{x=1}^A \beta_x^{(J)} = 1,$$

and by using corner constraints on the first differenced time parameters,  $\Delta J_2 = 0$  and  $\xi_2 = 0$ , resulting in a total of four constraints. This is enough to identify the drift  $d$  and the parameters of the mortality improvement rates  $Z_{x,t}$ , i.e.  $\beta_x, \beta_x^{(J)}, \Delta \kappa_t$ , and  $\Delta J_t$ . However, to identify the jump occurrences  $N_t$  and the autoregressive parameter  $a$ , we need to impose slightly stricter constraints. Details can be found in [Appendix 9.1](#).

It should be noted that these are not the only identification constraints that can be set. Given the recommendation by [Hunt and Blake \(2020\)](#), another possibility is to adopt a true normalisation scheme for the age parameters. That is, instead of a sum-to-one constraint, we could set the age parameters to have an Euclidean norm of one, that is

$$\|\beta_x\|_2^2 = \sum_{x=1}^A (\beta_x)^2 = 1 \quad \text{and} \quad \|\beta_x^{(J)}\|_2^2 = \sum_{x=1}^A (\beta_x^{(J)})^2 = 1.$$

The above identification can be achieved, for example, using **QR** decomposition, which results in two orthonormal age vectors that do not only have a norm of one, but are also orthogonal to each other, resulting in a dot product of zero, that is  $\sum_x \beta_x \beta_x^{(J)} = 0$ . When adopting the identification scheme using **QR**, the corner constraint on the time dependent parameters needs only to be set on the jump effect, thus  $\Delta J_2 = 0$ .

Both identification schemes have been successfully implemented and give unique parameter estimates. For sake of model comparison, we choose to go with the standard sum-to-one constraints, as these are the ones selected by [Liu and Li \(2015\)](#).

## 3.2 Priors

To estimate the parameters in Equation (3.2), we consider a Bayesian approach to inference. It is based on the idea of updating prior beliefs with the data at hand to obtain a posterior distribution of the parameters. For the selection of priors there are many options available. If not stated otherwise, we employ the use of so called weakly informative priors. Here, the prior should rule out unreasonable values but not be too restrictive so that it rules out plausible values.

As stated in Equation (2.3), we assume that the time-dependent parameter  $\kappa_t$  follows a random walk type representation, which we model using a normal prior:  $\Delta \kappa_t \stackrel{i.i.d.}{\sim} \mathcal{N}(d, \xi_t)$ . The jump effects are given a normal prior as well, such that,  $Y_t \stackrel{i.i.d.}{\sim} \mathcal{N}(\mu_Y, \sigma_Y)$ , while the jump occurrence is modelled using a Bernoulli distribution  $N_t \stackrel{i.i.d.}{\sim} \text{Bern}(p)$ . The age-specific parameters  $(\beta_1, \dots, \beta_A)$  and  $(\beta_1^{(J)}, \dots, \beta_A^{(J)})$  are given multivariate Dirichlet priors, which implicitly impose the sum-to-one constraints. The autoregressive parameter  $a$  is given a slightly informative Beta(1, 5) prior. This parameterisation favours smaller values of  $a$ , with the most prior mass around zero. Hence, there needs to be evidence by the likelihood to move the posterior estimate away from zero.

For the hyperparameters we choose a mix between weakly and informative priors. Starting with the jump probability we impose a more informative hyperprior, where  $p \sim \text{Beta}(1, 20)$ , which strongly favours small values of  $p$ . This is for the following reason. The parameter  $J_t$  is destined to model extreme events, not just noise. Thus, a shock should be something that occurs rarely, less than every few years, rather than some regular ups and downs. The latter type of effects should be captured by the noise term of the random walk coefficient and not considered a shock. When experimenting with uninformative hyperprior settings for  $p$ , we noticed the tendency of the model to obtain posterior estimates very close to one, resulting in two random walk parameterisations and a lack of convergence of the age-specific jump parameters  $\beta_x^{(J)}$ . Imposing a (weakly) informative prior on  $p$  alleviated the problem and helped with convergence.

Using our modelling approach, we want to capture shocks that have a positive (i.e. increasing) effect on death rates. Therefore, we assume that the jump mean parameter  $\mu_Y$  can only take on positive values and is given a half-normal prior. Another possibility is to give the jump effect  $Y_t$  itself a prior

distribution that has positive support only, such as the Gamma or Exponential distribution. However, the interpretation of the normal distribution using mean and standard deviation is much more straightforward and we wanted to compare our estimates with those of [Liu and Li \(2015\)](#). In addition, using a normal prior for  $Y_t$  resulted in better convergence. For the drift parameter  $d$  we assume a normal prior as well. This guarantees that  $\Pr(d \neq 0) = 1$ . Lastly, all standard deviations are given half-normal priors. An overview on specific values for the hyperparameters for each country can be found in the Appendix [9.4](#).

### 3.3 Parameter estimation

To estimate the parameters of our proposed model, we use NIMBLE ([de Valpine et al., 2017](#)), a system for programming statistical algorithms in R. NIMBLE provides a flexible and intuitive framework for model specification while supporting programming functions that adapt to model structures. Moreover, it allows for the selection of multiple samplers that include the well known MCMC methods as well as Hamiltonian Monte Carlo (HMC). For each parameter a different sampler can be chosen allowing for great flexibility and efficient computation. NIMBLE can be accessed via the *nimble* package in R ([de Valpine et al., 2023](#)). If not stated otherwise, NIMBLE uses the conjugate Gibbs samplers where possible as well as Metropolis-Hastings. However, the latter tends to be very inefficient due to the high autocorrelation of the samples. As a results we choose to change the samplers of multiple variables resulting in improved mixing performance. Moreover, to be able to use the flexibility of NIMBLE, we have chosen to parameterise the Dirichlet in terms of a normalised Gamma distribution, which allows us to select from a greater pool of available samplers, like the multivariate slice sampler of [Tibbits et al. \(2014\)](#) for example. A justification of the construction of a Dirichlet using the Gamma distribution can be found in the Appendix (see Section [9.2](#)). In addition, for the jump occurrence  $N_t$ , NIMBLE uses a special Gibbs sampler for binary-valued variables. A list can of the specific samplers for each parameter be found in Appendix [9.5](#).

To assess the convergence of all model parameters, we employ three widely recognised diagnostics: the split- $\hat{R}$  statistic as well as variants of the effective sample size, namely bulk effective sample size (Bulk-ESS) and tail effective sample size (Tail-ESS). These diagnostics are implemented using the *rstan* package ([Stan Development Team, 2023](#)), and for a more comprehensive discussion on their use, we refer to [Vehtari et al. \(2021\)](#).

In our analysis, we utilise two chains for each country and model. We discard the initial 5,000 iterations of each chain as “burn-in”, ensuring that the chains have stabilised. Subsequently, we draw an additional 10,000 samples per chain, with only every 10th sample being retained for inference. For a comprehensive understanding of parameter convergence and additional details regarding the MCMC settings, please refer to the Appendix.

### 3.4 Mortality forecasts

Since our model focuses on modelling mortality improvement rates, the forecasts generated by our model are also in the form of mortality improvement rates. However, to obtain forecasts of future (log) death rates, the mortality improvement rates can be transformed. Using Equation [\(3.1\)](#), we can calculate the death rate at time  $t + 1$  as follows:

$$\ln(m_{x,t+1}) = \ln(m_{x,t}) + Z_{x,t}. \quad (3.8)$$

Let the projection periods be denoted as  $h \in \{1, \dots, H\}$ . To generate a  $h$ -step ahead forecast of  $\ln(\hat{m}_{x,T+h})$ , we proceed by generating new values from our posterior predictive distribution for  $Z_{x,T+1}$ ,



$\dots, Z_{x,T+H}$  and apply Equation (3.8) recursively. This procedure can be repeated  $S$  times to obtain  $S$  draws from the posterior predictive distributions of  $\ln(\hat{m}_{x,T+h})$ . We can then derive prediction intervals using Monte Carlo simulations.

To make predictions for future values of  $Z_{x,T+1}, \dots, Z_{x,T+h}$ , we must also generate new values for time-dependent parameters. For example, to predict  $Z_{x,T+1}$ , we can follow these steps for each posterior draw ( $s = 1, \dots, S$ ):

*Step 1:* Generate new values of  $N_{T+1}^{(s)}$  by first drawing a value of  $p^{(s)}$  from the posterior distribution and then sampling  $N_{T+1}^{(s)}$  from a Bernoulli distribution with parameter  $p^{(s)}$ .

*Step 2:* Generate new values of  $J_{T+1}^{(s)}$ . Start by drawing  $\mu_Y^{(s)}$  and  $\sigma_Y^{(s)}$  from the posterior distribution. Then sample a new value of  $Y_{T+1}^{(s)}$  from a normal distribution with mean  $\mu_Y^{(s)}$  and standard deviation  $\sigma_Y^{(s)}$ . Afterwards, draw  $a^{(s)}$  and  $J_T^{(s)}$  from the posterior distribution. Use the newly generated  $N_{T+1}^{(s)}$  from Step 1 to compute a future value of  $J_{T+1}^{(s)}$ .

*Step 3:* Generate a new error term  $\varepsilon_{x,T+1}^{(s)}$  by sampling from a normal distribution with mean 0 and standard deviation  $\sigma_r^{(s)}$ .

*Step 4:* Obtain the  $s$ -th posterior draw for the remaining parameters and substitute all values into Equation (3.2) to generate  $Z_{x,T+1}^{(s)}$ .

## 4 In-sample comparison

To assess the in-sample fit of the models in question, we calculate the widely applicable or Watanabe-Akaike Information Criterion (WAIC; [Watanabe, 2010](#)). A lower WAIC value indicates a better-fitting model among the alternatives, as is the case with most information criteria. What distinguishes WAIC is its fully Bayesian nature, since it considers the entire posterior distribution for model evaluation. In addition to WAIC, the in-sample fit may be compared using cross validation.

Consider some data,  $\mathbf{y} = (y_1, \dots, y_N)$ , which is modelled as independent given the parameter  $\theta$ , hence  $p(\mathbf{y}|\theta) = \prod_{i=1}^N p(y_i|\theta)$ . A standard quantity in Bayesian analysis is the log predictive density (lpd),

$$\text{lpd} = \sum_{i=1}^N \ln p(y_i|\mathbf{y}) = \sum_{i=1}^N \ln \int p(y_i|\theta)p(\theta|y_i)d\theta.$$

To obtain an estimate of the lpd, we can use  $S$  samples from the posterior distribution, denoted  $\theta^{(s)}$  with  $s = 1, \dots, S$  to approximate the inner expectation:

$$\widehat{\text{lpd}} = \sum_{i=1}^N \ln \left( \frac{1}{S} \sum_{s=1}^S p(y_i|\theta^{(s)}) \right).$$

Using the lpd, we can calculate the WAIC by

$$\begin{aligned} \text{WAIC} &= -2\text{lpd} + 2p_{waic} \\ p_{waic} &= \sum_{i=1}^N V_{s=1}^S \left( \ln p(y_i|\theta^{(s)}) \right), \end{aligned}$$

where  $V_{s=1}^S (\ln p(y_i|\theta^{(s)}))$  denotes the posterior variance of the lpd for each data point  $y_i$  (Vehtari et al., 2017).

The Bayesian leave-one-out cross validation (LOO-CV) is based on the log predictive density given the data without the  $i$ -th data point  $p(y_i|y_{-i})$ . In practice, it is calculated as

$$\text{lpd}_{\text{loo}} = \sum_{i=1}^N \ln p(y_i|y_{-i}),$$

where

$$p(y_i|y_{-i}) = \int p(y_i|\theta)p(\theta|y_{-i})d\theta$$

denotes the leave-one-out predictive density without the  $i$ -th data point. In the above setting, exact cross validation would require refitting the model  $N$  times. However,  $p(y_i|y_{-i})$  can be approximated using importance sampling (Vehtari et al., 2017). A model with a higher  $\text{lpd}_{\text{loo}}$  indicates a better model fit by superior predictive performance. Oftentimes,  $\text{lpd}_{\text{loo}}$  is provided on the deviance scale, that is  $\text{LOO-CV} = -2\text{lpd}_{\text{loo}}$ , where a lower score suggests the better fit. Both the calculation of the WAIC and LOO-CV is implemented in the *loo* package in R (Vehtari et al., 2023).

## 5 Applications to real data

The data used for this study was sourced from the Human Mortality Database (HMD)<sup>1</sup> and Eurostat<sup>2</sup>. We focused on three western countries that experienced significant COVID-19 impacts, as indicated by deaths per 100,000 population<sup>3</sup>. Specifically, we analysed unisex populations from the United States (US), Italy, and Spain.

For Italy and Spain, we obtained data from Eurostat. To create a consistent dataset, we combined yearly death counts up to 2021 with provisional counts of weekly deaths for 2022, aggregating the latter to obtain annual death counts. Exposure data was available from Eurostat until 2022. In the case of the US, we acquired death and exposure counts up to 2021 from HMD. For the year 2022 we obtained provisional counts of weekly deaths from the National Center for Health Statistics (NCHS) that was downloaded from the Centers for Disease Control and Prevention (CDC) website<sup>4</sup>. As for the European data, the weekly counts were aggregated to obtain yearly counts of deaths. Mid year population estimates for the year 2022 was available from the United States Census Bureau<sup>5</sup>. To be able to combine multiple data sets by country we had to go with the lowest granularity regarding age group size. Provisional counts of deaths for US were given for age groups of width 10, except for the youngest age group. Hence, for sake of comparison, we choose to adopt this as the general age structure for all countries. Meaning that the data was organised into a total of  $A = 10$  age groups from ‘< 5’, ‘5-14’ up until ‘85+’.

Additionally, we used historical mortality data for the unisex population of England and Wales, covering the years 1901 to 2011, from the HMD website. This dataset featured a slightly different age

<sup>1</sup>HMD website: <https://www.mortality.org/>

<sup>2</sup>Eurostat website: <https://ec.europa.eu/eurostat/de/web/main/data/database>

<sup>3</sup>COVID-19 data: <https://coronavirus.jhu.edu/data/mortality>

<sup>4</sup>CDC data: <https://data.cdc.gov/NCHS/Provisional-COVID-19-Death-Counts-by-Age-in-Year-3apk-4u4f>

<sup>5</sup>US Census Bureau data: <https://www.census.gov/data/tables/time-series/demo/popest/2020s-national-detail.html>

group structure, ranging from ‘< 1’, ‘1-4’, ‘5-14’, ‘15-24’, and so on up to ‘75-84’. The variation in age group structure enabled us to compare the fit and parameter estimates of our model with those of [Liu and Li \(2015\)](#), as this dataset aligns with one of the datasets reviewed in their work. A summary of the data sources can be found in [Table 1](#).

Table 1: Sources of mortality data

Country	Year	Source
<b>Counts of Death</b>		
England and Wales	1901 - 2011	HMD
Italy	1980 - 2022	Eurostat
Spain	1980 - 2022	Eurostat
United States	1980 - 2021	HMD
	2022	NCHS
<b>Population Estimate</b>		
England and Wales	1901 - 2011	HMD
Italy	1980 - 2022	Eurostat
Spain	1980 - 2022	Eurostat
United States	1980 - 2021	HMD
	2022	US Census Bureau

## 5.1 Analysis of England and Wales data during the world wars

To start our analysis, we applied both our model and a Bayesian implementation of the approach presented by [Liu and Li \(2015\)](#), hereafter referred to as the Liu-Li model, to historical mortality data spanning from 1901 to 2011 for the unisex population of England and Wales. The occurrence of the jumps, in terms of mean estimates for  $N_t$ , is visually depicted in [Figure 1](#). Herein lies an advantage of the Bayesian approach, since the jump occurrences  $N_t$  are treated as a parameter instead of a random variable. This allows us to detect the specific years which the model flags as jumps, instead of just having an estimate of the jump probability. As anticipated, both models identified the same periods coinciding with the two World Wars (WWI, 1914 - 1918; WWII, 1939 - 1945) as mortality jumps. During the period around the First World War, specifically from 1914 to 1919, our Model indicated a 100% probability of jump occurrence, as evidenced by posterior mean estimates for  $N_{1914}, \dots, N_{1919}$ . Notably, the jump in 1919 can be attributed to the Spanish flu, a well-documented historical event. Similarly, around the time of the Second World War, covering the years 1940 to 1945, our model estimated these as shock years based on  $N_{1940}, \dots, N_{1945}$ . It is important to mention that the United Kingdom officially entered World War II in September 1939, with major battles commencing in 1940.

### 5.1.1 Parameter estimates of the Liu-Li Model

Starting with the Liu-Li model, we observed remarkably consistent parameter estimates when compared to the frequentist approach of [Liu and Li \(2015\)](#) as depicted in [Figure 2](#). Notably, our Bayesian estimates exhibited posterior means and standard deviations that closely aligned with the mean and bootstrapped standard deviation of their frequentist model. Of interest was the divergence between the two approaches

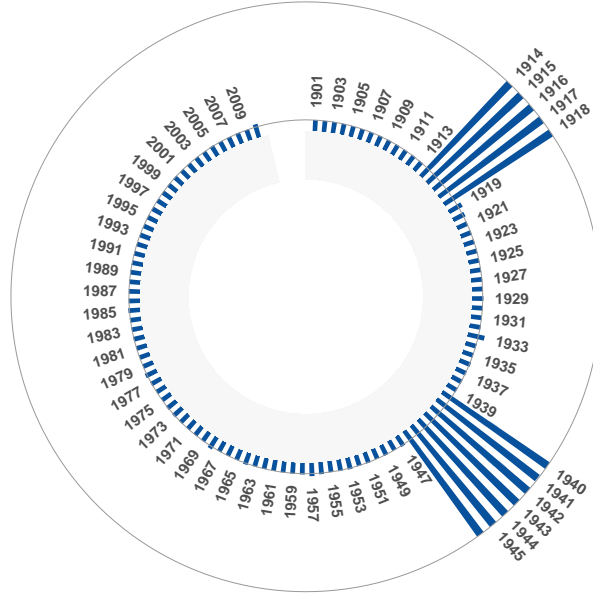


Figure 1: Posterior mean estimates of own model for all  $N_t$ . Outer line denotes a value of one while the inner line a value of zero.

concerning the jump intensity parameter,  $\mu_Y$ , and the standard deviation,  $\sigma_Y$ . The Liu-Li model produced a posterior mean of  $\mu_Y$  at 2.92 (80% PI: [2.28, 3.54]) and  $\sigma_Y$  at 1.63 (80% PI: [1.21, 2.13]), both surpassing the estimates of [Liu and Li \(2015\)](#). This discrepancy might be attributed to the influence of Bayesian prior information in the context of limited data, potentially impacting the posterior estimates. The standard deviations associated with the jump effects,  $\mu_Y$  and  $\sigma_Y$ , exhibited significant uncertainty in both the Bayesian and frequentist approaches. The bootstrapped standard deviations from [Liu and Li \(2015\)](#) showed a similar level of variation for both parameters, reflecting the inherent challenge of estimating parameters from a limited number of data points, particularly in the context of few jump years. This uncertainty appears to be a shared characteristic between frequentist and Bayesian methods.

### 5.1.2 Comparison of the Liu-Li model and our model

We now look at the parameter estimates of our vanishing jump approach and compare these with the (Bayesian) Liu-Li model. Our estimates are very similar to those of the Liu-Li model. The approaches only differ substantially in the posterior estimates of  $\mu_Y$  and  $\sigma_Y$ , where both parameters have higher posterior means in the Liu-Li model. In our model  $\mu_Y$  has a posterior mean of 2.21 (80%-PI [1.58, 2.86]), while that of  $\sigma_Y$  is 1.66 (80%-PI [1.24, 2.15]). For the vanishing parameter  $a$ , our model estimates the posterior mean to be 0.24 (80% PI: [0.20, 0.26]), which can be considered a medium sized effect. Intuitively, it is plausible, that a lingering effect can be observed even after the war has ended, whether through reduced economic activity resulting in a lower standard of living, or through injuries sustained during the war that continue to affect people afterwards and may lead to a premature death. Moreover, looking at the posterior estimates of  $\beta_x^{(J)}$  (cf. Figure 2) the shock of the war is mostly affecting young people, that is age groups of 15-24 and 25-34. Posterior estimates including measures of convergence of all parameters can be found in the Appendix in Table 4.

In our analysis of the England and Wales data, our proposed model demonstrates a lower WAIC and

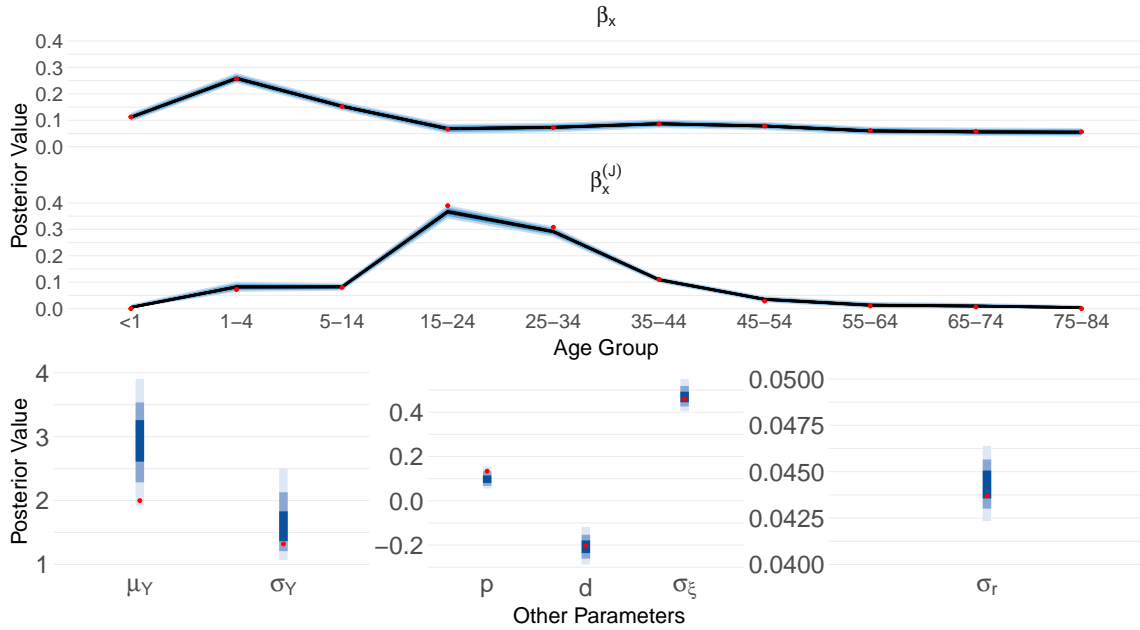


Figure 2: Posterior estimates of the Liu-Li model for England and Wales of all parameters. Different shades denote the 50-%, 80-% and 95-% posterior intervals where the width of the interval is sorted from dark to light. The red dots denote mean estimates of the frequentist approach of [Liu and Li \(2015\)](#).

LOO-CV value compared to the Liu-Li model. Results are given in [Table 2](#). This outcome underscores the enhanced in-sample fit achieved by incorporating a vanishing effect parameter  $a$  in our model proposition. The observed improvement signifies the ability of our model to capture the complex dynamics of mortality rates during the war events in this case more accurately than the Liu-Li model, resulting in a more favourable fit to the available data.

Table 2: In-Sample comparison of the Liu-Li and our model on England and Wales data during the world wars. Bold value denotes best of the column.

Model	LOO-CV	WAIC
Own	<b>-3476.56</b>	<b>-3502.92</b>
Liu-Li	-3472.61	-3500.38

## 5.2 Analysis of data during the COVID-19 pandemic

Our primary objective is to introduce an enhanced Lee-Carter model capable of accurately capturing the fluctuations in log death rates driven by the COVID-19 pandemic. The classical approach of assessing predictive accuracy through data splitting faces unique challenges in our context. The pandemic predominantly impacts the most recent years of data, making it impractical to exclude these years and estimate parameters using only the earlier data. Such an approach would overlook the pandemic’s specific dynamics.

Given these challenges, our analysis focuses solely on evaluating the in-sample fit of our models. To demonstrate the effectiveness of our refined Lee-Carter model, we will showcase its performance in

three distinct countries: the United States, Spain, and Italy. These countries were chosen as illustrative examples due to their significant experiences with the COVID-19 pandemic and the availability of relevant mortality data. In the following sections, we will delve into the model’s parameter estimates and its capacity to capture the unique mortality patterns observed during the pandemic in each of these nations.

### 5.2.1 United States

We applied our model to the US mortality data spanning from 1980 to 2022, comparing it with the Liu-Li model. Initially, we ensured that all model parameters had converged successfully, as confirmed by both the split- $\hat{R}$  and effective sample size metrics. The model demonstrated remarkable confidence in its assessments of the data for 2020 and 2021, with posterior mean estimates of  $N_{2020}$  and  $N_{2021}$  equalling 1 and a posterior standard deviation of 0. This high level of confidence indicates that the model considered these years as shock years with absolute certainty. Conversely, the other years showed extremely low to negligible posterior means, making them unsuitable candidates for jump years in the model. For an overview on the estimated occurrences of jump years see panel a) of Figure 3.

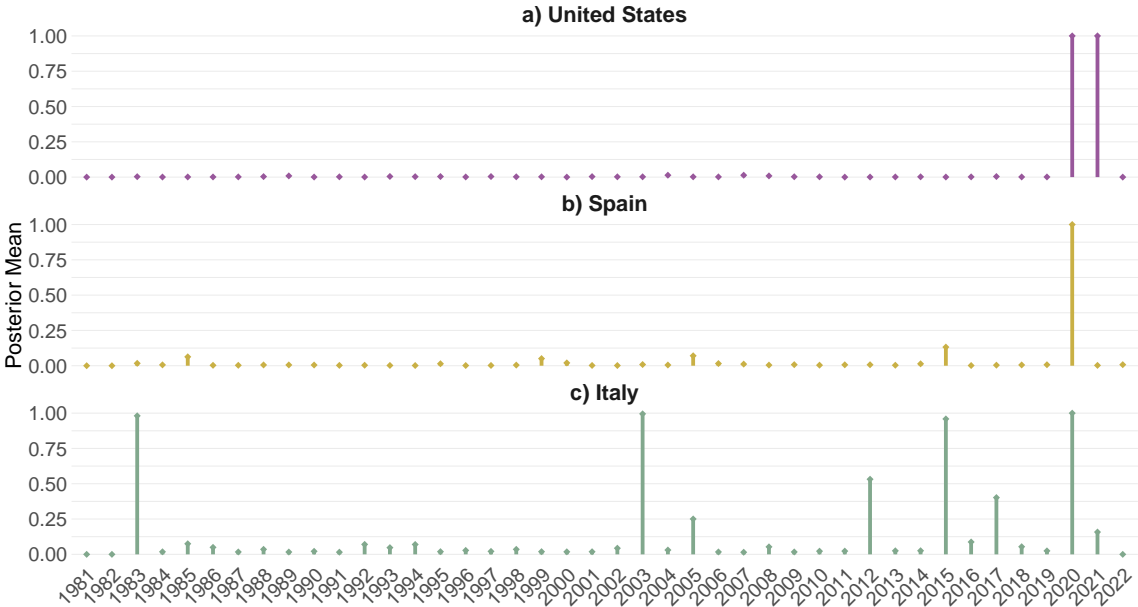


Figure 3: Comparison of posterior mean estimates for  $N_t$  across time for all countries.

Given the inherent similarity between our model and the Liu-Li model, the parameter estimates aligned closely for most aspects. Still, notable distinctions emerged in the context of the “shock” parameters, particularly the jump intensity parameters,  $\mu_Y$  and  $\sigma_Y$ . In our model, these parameters yielded slightly lower posterior mean estimates, with values of 1.38 (80%-PI [0.64, 2.07]) and 0.94 (80%-PI [0.24, 1.90]), respectively, compared to 1.46 and 0.99 in the Liu-Li model. It’s worth acknowledging the relatively large standard deviation in the estimates. This variability is not unexpected, as the model predominantly considers only two years extreme events, meaning that parameter estimation is based on these two years only. Furthermore, in such data-scarce scenarios, the prior distribution significantly influences posterior estimates, especially via the choice of hyperparameters.

Interestingly, the Liu-Li model predicts 2022 to be a shock year with hundred percent certainty. However, it is important to mention, that the estimated intensity, i.e.  $Y_{2022}$ , is around half as big as it

has been for the year before. This suggests that the effect of the pandemic is still present in 2022, but has decreased significantly. Although our model did not predict the year 2022 to be another shock year, it is able to accurately estimate the effect on the mortality rates using the vanishing effect parameter  $a$ , which exhibits a posterior mean of 0.45 (80%-PI [0.35, 0.55]). This is in line with the result of the Liu-Li model, which estimated that the 2022 shock is about half as large as the one of the preceding year. One might argue that our model proposition is not necessary in this case, since the Liu-Li model can accurately capture the substantial effect. However, this is not entirely true, as the inclusion of another year with considerably lower intensity has the potential to affect the estimates  $\mu_Y$  and  $\sigma_Y$ . All posterior estimates of our model can be found in Figure 4 and Table 5 in the Appendix.

Irrespective of the model choice, the posterior mean estimates of  $\mu_Y$  and  $\sigma_Y$  underscore the substantial impact of the COVID-19 pandemic on mortality rates in the US. However, this influence appears to be more diffuse, affecting a broader age spectrum rather than concentrating on specific age groups. Intriguingly, the mortality jump pattern, as represented by  $\beta_x^{(J)}$ , exhibits a plateau in the middle age range (from 15-24 to 45-54), with a milder impact observed at higher ages. This pattern aligns with findings from Faust et al. (2022), which revealed the most significant relative increase in mortality among the 18-49 age group, corresponding to the working population that played a central role in the spread of COVID-19 (Monod et al., 2021).

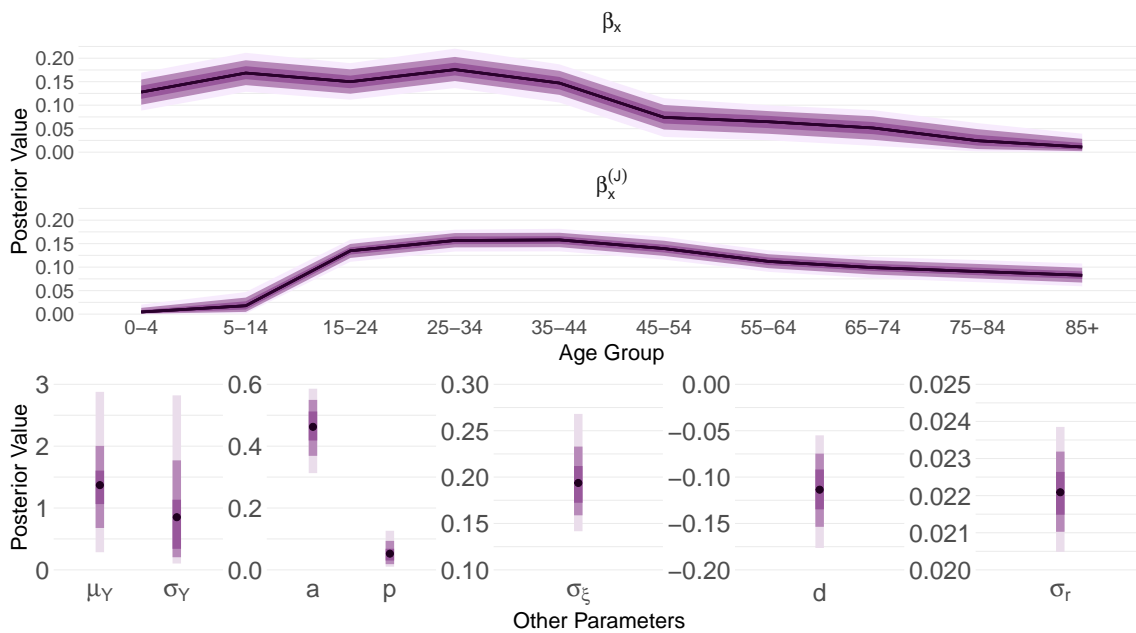


Figure 4: Overview on posterior estimates of all parameters for the US using our model. Different shades denote the 50-%, 80-% and 95-% posterior intervals where the width of the interval is sorted from dark to light. The dark purple line respectively point denotes the posterior mean.

When evaluating the goodness of fit using the WAIC metric, our proposed model demonstrates a superior performance compared to the Liu-Li model (see Table 3). However, the difference is not massive, which is not unexpected given that the two models diverge mainly over a period of two years, i.e. 2021-2022. It's worth noting that this small divergence might downplay the model differences in the immediate context. However, as an additional year's data becomes available, the distinction could become more pronounced. This is due to the persistent impact of the 2020 and 2021 shocks in our model, even if no explicit jump is recorded in the future. The cumulative effect underscores the potential for our model

proposition to capture the lasting influence of pandemic-induced dynamics.

Table 3: In-sample fit comparison of the Liu-Li and own model on COVID-19 data for multiple countries. Bold value denotes best of the column.

Model	Italy	Spain	US
<i>WAIC</i>			
Own	<b>-1447.75</b>	<b>-1497.44</b>	<b>-1882.69</b>
Liu-Li	-1446.94	-1491.02	-1879.81
<i>LOO-CV</i>			
Own	<b>-1442.74</b>	<b>-1491.07</b>	<b>-1873.04</b>
Liu-Li	-1440.01	-1483.61	-1869.96

### 5.2.2 Spain

Both the Liu-Li as well as our approach estimate the posterior probability of a jump occurring in 2020, i.e.  $N_{2020}$  to be one, while most of the other years, including 2021, have a negligible posterior mean estimate close to zero. Thus, contrary to the United States, the COVID-19 pandemic in Spain is a one-period shock only. An overview on the jump occurrences for Spain can be found in panel b) of Figure 3. However, this does not mean that the effect of the pandemic disappeared in 2021. The vanishing effect  $a$ , has a posterior mean of 0.22 (80%-PI [0.08, 0.36]), indicating a medium sized effect. This means, that that on average 22% of the shock in 2020 is still present in 2021.

Looking at the other posterior estimates of our model, we observe medium size estimates of the shock parameters. The posterior mean estimate of  $\mu_Y$  is given by 1.05 (80%-PI[0.29, 1.97]), while that of  $\sigma_Y$  is 0.93 (80%-PI[0.32, 1.69]). Admittedly, both parameters have rather large posterior intervals, which can be attributed to the single shock period. Again, with more and potentially corrected data available the uncertainty of these estimates can be reduced.

Looking at the other parameters, it is clear that the COVID-19 pandemic had a greater impact on older age groups than on younger ones. Two notable things are seen for the posterior estimates of  $\beta_x^{(J)}$ . First, similar to the United States, there is a small plateau in the posterior mean of the middle ages. However, the posterior mean then decreases, only to increase again at older ages, reaching its global maximum for the age group 75-84. Thus, both the mortality rates of the medium aged as well as the elderly were affected most by the COVID-19 pandemic. Posterior estimates of all parameters including uncertainty quantification can be found in Figure 5.

Comparing the model fit of Liu-Li and our model using the WAIC and LOO-CV, we see a superior performance of our approach (cf. Table 3). Although the uncertainty in the vanishing parameter  $a$  is quite high, it seems like the impact of COVID-19 does not completely disappear after 2020, but still affects the years 2021 and 2022. Adding this slowly vanishing structure to the model helps at describing the data and subsequently leads to a better fit.



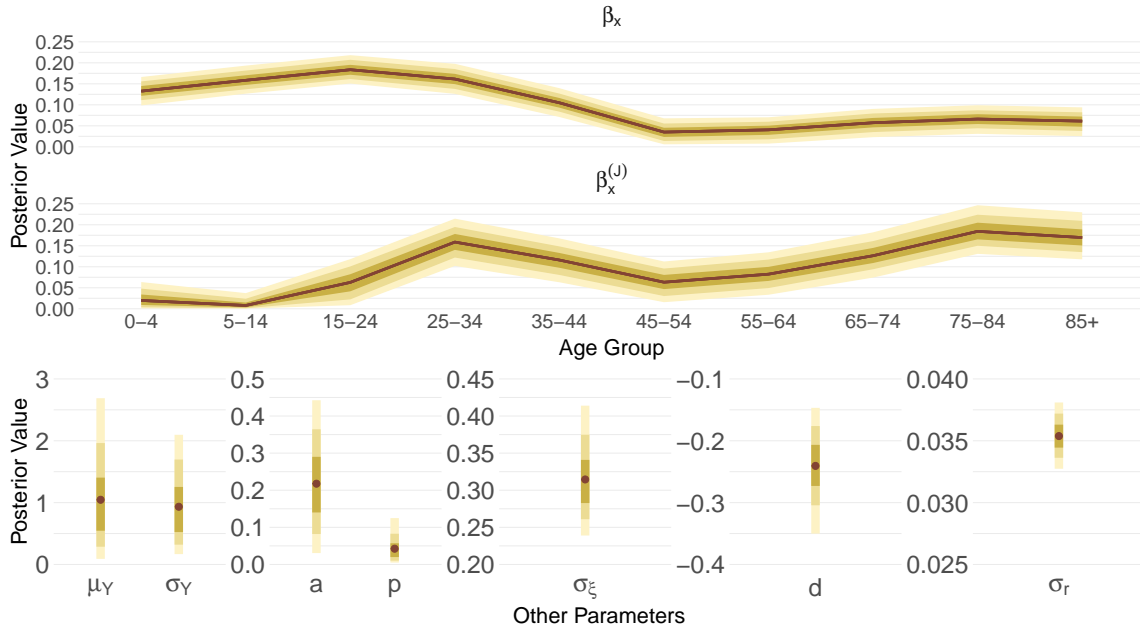


Figure 5: Overview on posterior estimates of all parameters for Spain using own modelling approach. Different shades denote the 50-%, 80-% and 95-% posterior intervals where the width of the interval is sorted from dark to light. The brown line and points denote the posterior mean.

### 5.2.3 Italy

For Italy, we obtain mixed results. First, both the Liu-Li as well as our own modelling approach estimate several other years besides 2020 as jump years (see panel c) of Figure 3). In particular, the years 1983, 2003 and 2015 are considered shock years with 100%-certainty. While for 2017 and 2012 there exists some evidence of a shock. In 1983 and 2003, two heat waves struck Italy. Although there is limited research on the precise influence of the former heat wave on mortality rates, the Centers for Disease Control and Prevention have noted its effects (CDC, 1984). In contrast, the impact of the latter heat wave has been more thoroughly investigated. In 2003 the south of Europe (especially France and Italy), experienced what were then record-breaking temperatures. Especially the north of Italy was affected heavily. For ages 75+ recorded deaths between June 1st and August 31th increased by 21.3% compared with the same time period of the year before (Conti et al., 2005). The year 1983 could have had a similar effect to that of 2003. Moreover, as heat waves become more likely and more extreme, it is entirely possible that these effects will become more pronounced and occur more frequently in the future. Next to heat waves, cold spells, i.e. extremely low temperatures in the winter, can affect yearly death rates as well. In 2012, Italy was hit by an exceptional cold spell increasing respiratory and cardiovascular diseases among the old people (de'Donato et al., 2013). The peaks in 2015 and 2017 may be explained by an influenza epidemic in Italy, with high excess deaths registered especially among the elderly (Rosano et al., 2019).

Given that several years were labelled as shock years, it is reasonable to assume that not all of them had an equally extreme impact on the mortality rate. This aligns with our model's results, where the estimated shock intensity  $\mu_Y$  has a posterior mean 0.32 (80%-PI[0.17, 0.47]) while that of  $\sigma_Y$  is 0.24 (80%-PI[0.10, 0.41]). Furthermore, the vanishing parameter  $a$  is estimated to be the smallest, with a mean of 0.16 (80%-PI[0.02, 0.34]), suggesting that the shocks quickly vanish in the subsequent periods. Especially for the heat waves and cold spells, this is a realistic scenario.

The age pattern of the shock, as seen by the estimates of  $\beta_x^{(J)}$ , suggest that the mortality shocks affect mostly older people. The posterior estimate of  $\beta_x^{(J)}$  is lowest for age group 15-24 and then continuously increases to be highest for the two oldest age groups. This is in line with the findings of other researchers, that the peaks in mortality due to heat waves, cold spells and influenza pandemics were mostly affecting the elderly population. An overview of the posterior estimates of all parameters can be found in Figure 6.

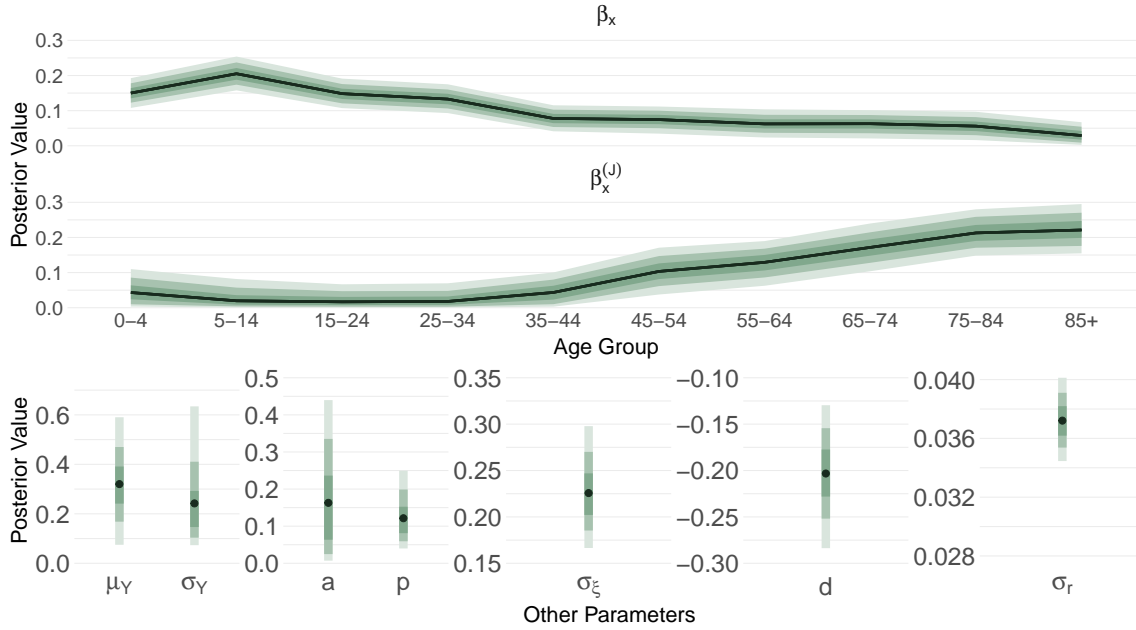


Figure 6: Overview on posterior estimates of all parameters for Italy using own modelling approach. Different shades denote the 50-%, 80-% and 95-% posterior intervals where the width of the interval is sorted from dark to light. The dark green line respectively point denotes the posterior mean.

Looking at the in-sample fit, using the WAIC and LOO-CV criteria, it can be seen that our model and the Liu-Li approach have a comparable fit (cf. Table 3). Nonetheless our model performs slightly better. However, the difference, especially in terms of WAIC, is only marginal and can be explained by the small value of  $a$  making our model and that of Liu and Li very similar.

### 5.2.4 Country-specific analysis and comparisons of pandemic effects

Comparing posterior parameter estimates across various countries provides insights into the extent of their exposure to the COVID-19 pandemic. A compelling example is illustrated in Figure 7, where the jump probability for multiple countries is depicted. Notably, Italy exhibits the highest posterior mean in jump probability, trailed by the US and Spain. This observation implies that the model identifies a larger number of years as shock years in Italy compared to Spain and the US, which was observed in Figure 3.

Furthermore, leveraging the estimated vanishing effect parameter  $a$ , we can assess the pace of recovery from shocks across countries. As demonstrated in Figure 8, a distinct recovery pattern emerges for each country. In the case of Spain, the posterior estimate is moderate, whereas for the United States, it can be considered high. The latter is primarily due to persistent impact of COVID in 2022. The data indicates, that Spain has undergone a more rapid recovery, while the United States continues to face increased mortality due to COVID-19 even in later years. On the contrary, Italy has displayed the swiftest recovery, evident in its lowest posterior mean and a posterior mode (MAP) of 0.03, which is very close to

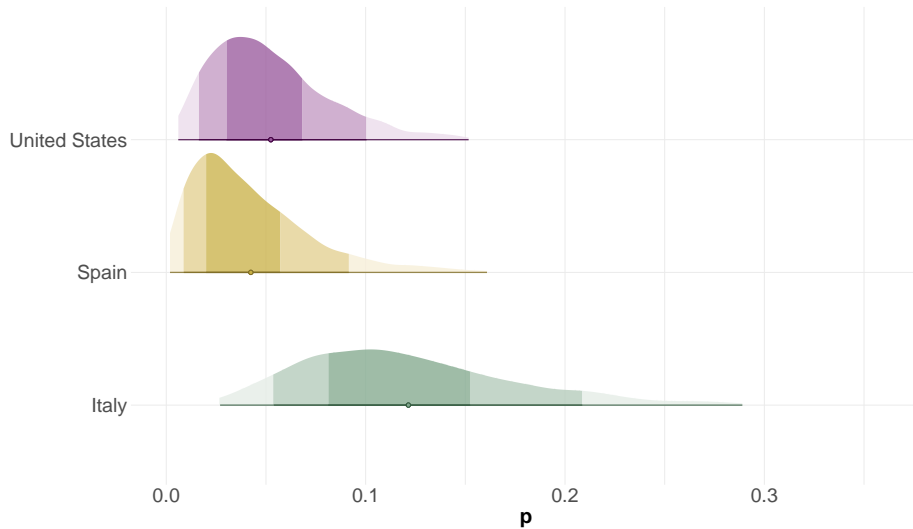


Figure 7: Comparison of posterior jump probability  $p$  across countries. For each country there are three different shades denoting the 50-%, 80-% and 99-% posterior intervals where the width of the interval is sorted from dark to light. Below the density, there is a single point representing the posterior mean.

zero. However, the vanishing parameter  $a$  represents multiple effects. Those of heatwaves, where small values of  $a$  are likely, as well as the influence of multiple influenza seasons and the COVID pandemic. Consequently, the posterior distribution consists of an average or mixture of two types of effects, making it difficult to compare the pace of COVID recovery to that of the other two countries. The uncertainty associated with the estimation of  $a$  is pronounced for all countries, manifested by broad posterior intervals. This uncertainty is attributed to the limited number of available pandemic data points, accentuating the importance of considering a Bayesian approach that accommodates uncertainty.

It's noteworthy that despite this moderate uncertainty in specific values of  $a$ , the WAIC and LOO-CV scores consistently favour our model proposition over the Liu-Li model for all three countries. This underscores the significance of incorporating the vanishing effect parameter within the model, even in cases where uncertainty about its precise value exists. The in-sample based comparison demonstrates that the model's predictive capabilities benefit from the inclusion of the vanishing effects parameter, outweighing the challenges posed by limited data points and associated uncertainty.

Furthermore, the shock pattern exhibited by  $\beta_x^{(J)}$  reveals distinct variations across different countries. To illustrate, in Italy, the shock predominantly affects the older population, whereas in the United States, the impact is distributed across a wide range of age groups, displaying a pronounced peak within middle age groups, as indicated by the posterior estimates. Spain occupies an intermediate position between the aforementioned patterns. This variance is visually depicted in Figure 9, where the posterior mean shock pattern, along with its 80%-PI, is depicted for each country across all age groups.

Additionally, the intensity of the shock is most pronounced in the United States, in comparison to the other countries. This is visually evident in Figures 4, 5 and 6, where the posterior estimates of the shock parameters  $\mu_Y$  and  $\sigma_Y$  are included for each country. These figures emphasise that the magnitude of mortality impact during a jump event is most substantial in the US, underscoring the heightened sensitivity of the mortality rates to pandemic-related shocks in that country.

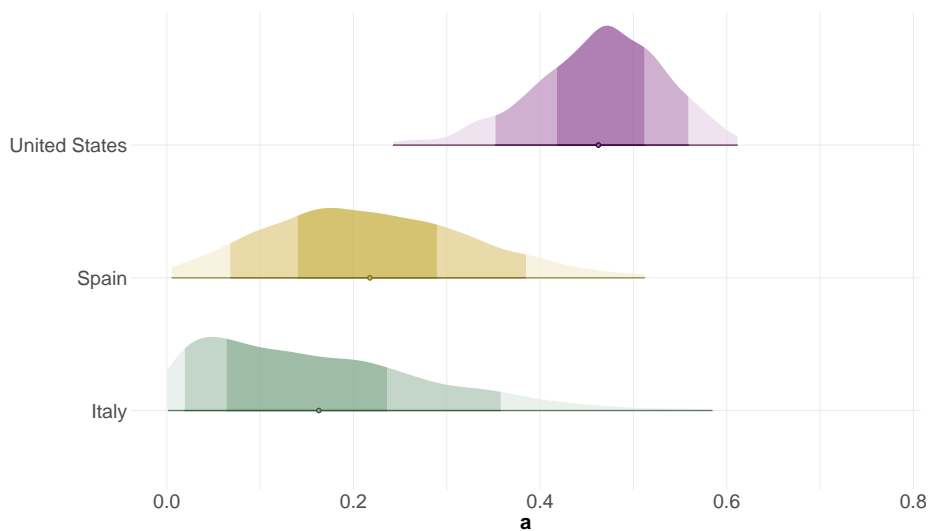


Figure 8: Comparison of the posterior vanishing parameter  $a$  across countries. For each country there are three different shades denoting the 50-%, 80-% and 99-% posterior intervals where the width of the interval is sorted from dark to light. Below the density, there is a single point representing the posterior mean.

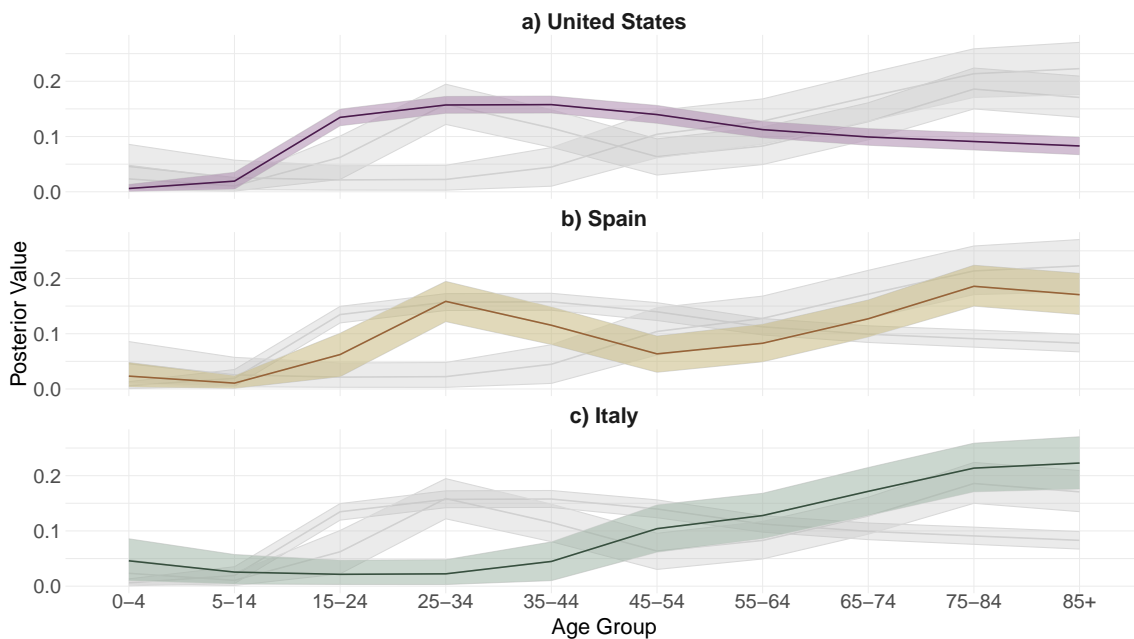


Figure 9: Posterior estimates of Jump effect  $\beta_x^{(J)}$  for each country. Thick line denotes posterior mean while the shades denote 80%- posterior intervals. Gray shaded area shows respective estimates of the other countries.

## 6 Forecasting

### 6.1 Prediction of mortality rates

Following the methodology of Section 3.4, we can forecast future mortality rates recursively by application of Equation (3.8). In Figure 10, forecasted mortality rates are shown for the middle age groups, that is age groups 45-54 up until 75-84 for Spain. The plot displays a mean forecast next to 90%, 95% and 99% prediction intervals. These are calculated empirically based on 2000 generated trajectories, where for each draw from the posterior a future path was forecasted.

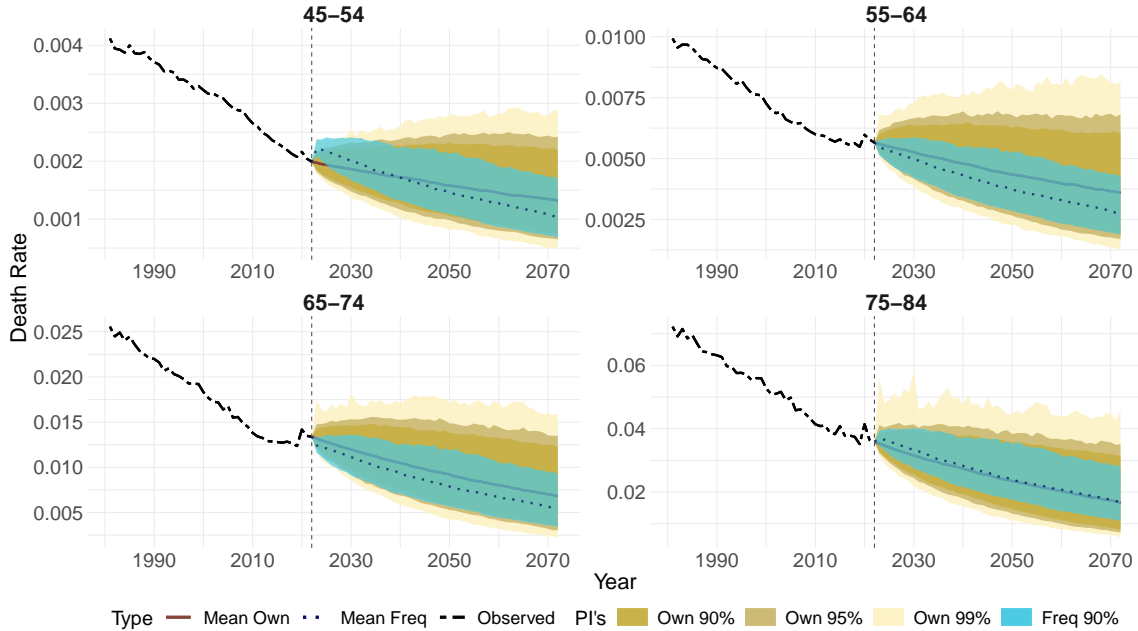


Figure 10: 50-year ahead forecasts of death rates for different age groups of Spain including prediction intervals (PI) using both a frequentist LC (Freq) and own model (Own). Dashed black line denotes actual observed values, while dotted blue line denotes the mean forecast (Mean Freq) of the LC model and solid brown the mean forecast (Mean Own) of own model. Moreover, the different shades denote the respective prediction intervals of own and the frequentist model.

To compare the width of the prediction intervals, we have fit a frequentist LC model on the same data using the “StMoMo” package (Villegas et al., 2018) and added the mean forecast as well as 90% prediction intervals to the plot. It can be seen, that the 90% prediction interval of our approach is only slightly bigger than the counterpart of the frequentist method. Especially for medium-term forecasts, i.e. up to 15 years, we do note 90% intervals of similar width. Thus, it can be concluded, that our method does not produce unreasonable wide prediction intervals, even though it specifically allows for the possibility of future shocks.

### 6.2 Measuring the shock effect by age groups

After having estimated all the parameters we were able to forecast future death rates. Moreover, we can calculate how much future death rates are affected by the addition of the age-specific jump effect  $\beta_x^{(J)} J_t$ . Using draws from the posterior predictive distribution we can calculate empirical quantiles for the shock

component  $\beta_x^{(J)} J_t$  to answer the question of how much of a percentage increase in death rates is likely to occur in the future due to a shock.

Hereby, consider that the log death rate of our model consists of the log death rate of a LC model, i.e. a scenario without a jump, denoted  $\ln(m_{x,t}^{LC})$ , plus the shock component  $\beta_x^{(J)} J_t$  in case there is a jump:

$$\ln(m_{x,t}) = \underbrace{\alpha_x + \beta_x \kappa_t + e_{x,t}}_{\ln(m_{x,t}^{LC})} + \underbrace{\beta_x^{(J)} J_t}_{\ln(c)}. \quad (6.1)$$

Using basic rules of logarithms, we can calculate the percentage increase induced by the shock component to the death rate of a jump free scenario, with

$$m_{x,t} = m_{x,t}^{LC} \cdot c. \quad (6.2)$$

In Figure 11, we have plotted 90%, 95% and the 99% quantile of the predicted percentage increase  $c$  by age group for each country. In addition we have added a dashed line showing the actual, observed increase to the death rates from due to the COVID-19 pandemic. Here, we have taken the average age specific death rates from 2016 to 2019 and calculated by how much this average was increased (or decreased) in 2020. We note that this increase is given in percentages, not percentage points.

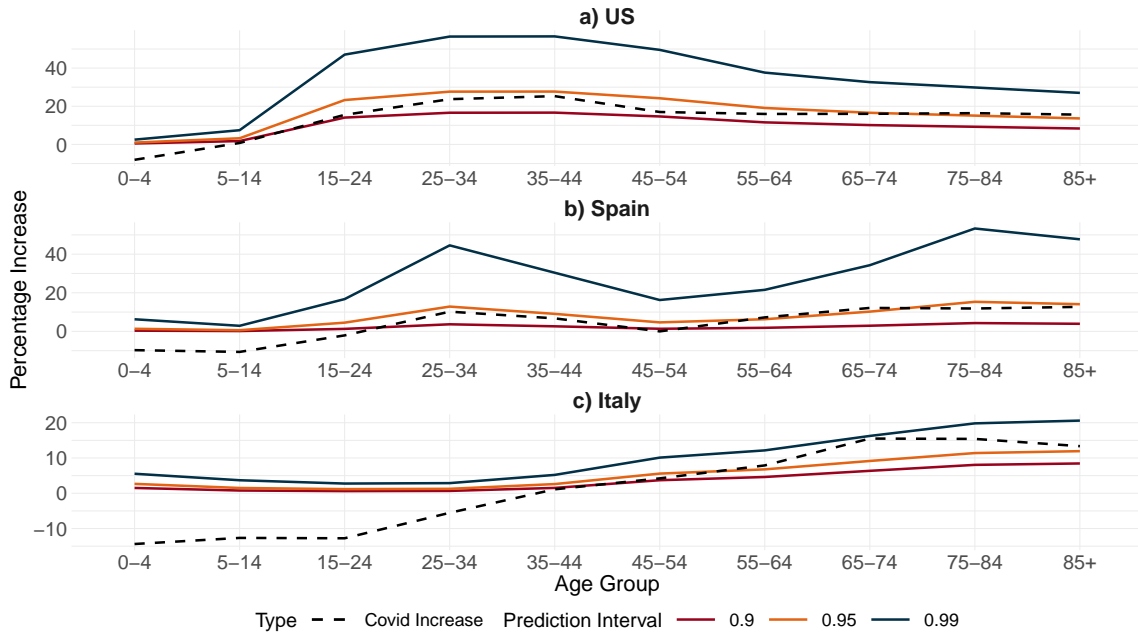


Figure 11: Observed percentage increase in death rates from the average of 2016 - 2019 to 2020 by countries (Covid Increase). Solid lines denote the respective upper bound of the prediction interval for  $c = \beta_x J_t$ .

First, looking at Figure 11 we can see that the COVID-19 pandemic did not induce a parallel constant shift to the log death rates, as some authors (e.g. Schnürch et al., 2022) proposed. Adding a constant to all age-specific log death rates would result in a constant percentage increase of the mortality rates, which is not observed. Second, using Figure 11, we can provide an upper bound on the increase in mortality rates that our model predicts for a future time period. For example, our model states that for any future single year, the mortality rates for the age group 75-84 in Spain will not increase by more than 10% with

a probability of 95%. However, we are aware that it is difficult to draw general conclusions for a future pandemic after having observed just one. The results should not be considered an attempt to forecast the severity of a future pandemic but rather as a tool to better visualise and capture the impact of the mortality shocks in the past.

## 7 Conclusion

In this paper we have introduced a new model that allows for more accurate modelling of mortality rates in the event of a shock. More precisely, we have extended the well-known LC model structure to allow for the inclusion of a vanishing or diminishing effect, where the effect of a shock is largest at the beginning and then gradually diminishes over time. Compared with the approach of [Liu and Li \(2015\)](#), our model better captures the underlying pattern of the COVID-19 pandemic for Spain, US and Italy. However, in the case of Italy, the advantage of our model is less pronounced due to the presence of heat waves that do not present slowly vanishing effects, which tends to favour the Liu-Li model. Additionally, we have demonstrated that the jump auto-correlation structure is applicable to various shock scenarios, as evidenced by the improved in-sample fit in the case of war-related data in England and Wales. In summary, our model offers the greatest benefit in single-period wave scenarios with a gradually vanishing effect. However it is also suitable in other scenarios, such as multi-period jumps observed in the US and during the world wars in England and Wales.

A valid point of criticism, nonetheless, relates to the considerable variability observed in the jump parameters, namely  $\mu_Y$ ,  $\sigma_Y$ , and  $a$ . Employing a Bayesian hierarchical modelling approach could potentially reduce this variability by pooling information across dimension. However, the general problem remains: No matter the approach, the model will have difficulty in estimating the parameters with only a few data points available, as evident by comparable levels of uncertainty observed in a frequentist analysis of the England and Wales data by [Liu and Li \(2015\)](#). Though, with the availability of an increased number of time points a substantial reduction in the standard deviation will be achieved. For example, for England and Wales, the standard deviation of the vanishing parameter  $a$  is moderate. This trend highlights that our method's efficacy is most pronounced when a larger temporal scope is available, enabling more robust estimation of the parameters. In essence, the improved estimation of  $a$  for England and Wales, directly corresponds to the accrual of more post-COVID data, underscoring the benefits of our approach as the dataset expands over time.

On the other hand, an advantage of the Bayesian approach that we have not explored further is the use of expert opinion for the specific choice of hyperparameters in prior distributions. For example, [Zhou and Li \(2022\)](#) incorporates expert opinion to simulate future mortality scenarios for events similar to the COVID outbreak. The same expert opinion could be used to set more informative priors, exploiting the interplay between prior and likelihood to update the posterior. In data-rich scenarios the estimates are primarily influenced by the data, whereas in data-scarce settings, the influence of the prior, or expert opinion, becomes more pronounced. This approach may substantially reduce the posterior variability and can be seen as a middle ground between purely expert based and data-only estimation.

Moreover, our model assumes that after a shock, the trend of mortality rates tends to return to their pre-shock trend driven by their constant drift. However, it is also possible that the shock has introduced either a new trend or baseline level. For example, after a severe pandemic, the population may be more alert to infectious diseases, leading to greater caution during the winter months. This change in behaviour could lead to lower levels of mortality after the pandemic. On the contrary, the impact might decrease but not disappear completely. Rather it could converge toward a general baseline level, which results in a permanent effect that can be compared to other causes of death such as the flu. Such scenarios which

are briefly discussed in [van Berkum et al. \(2022\)](#) are not considered by our approach but can constitute an interesting generalisation of our model.

Furthermore, the shock of a pandemic's mortality can trigger a compensatory response. There is an argument that a pandemic accelerates the demise of those already in poor health. This type of scenario, while not observed, was especially discussed at the beginning of the COVID-19 pandemic (e.g. [Cairns et al., 2020](#)). Here it is believed that many of those who die during a pandemic would have died anyway in the near future, resulting in a slight decrease in the mortality rates among survivors. This contradicts our assumption of a pandemic effect that slowly vanishes over time, making our model unsuitable for this type of scenario.

So far, only the in-sample fit of our model has been evaluated and compared with that of competing models. This is due to the recent occurrence of the COVID-19 pandemic. However, in the future as more data become available, the out-of-sample performance should be considered as well.

In practical applications, our model holds promise for actuarial contexts, particularly in determining solvency capital for mortality and longevity risk, which is imposed by supervisory authorities. The wider confidence intervals provided by our approach suggest that insurance companies may need to increase their capital reserves to safeguard against future pandemics and mortality shocks. This highlights the real-world significance and potential impact of our modeling framework on risk management in the insurance industry.

## 8 Data availability

For full replication of the results, we provide the code including data at our GitHub repository, available at <https://github.com/goesj/VanishingJumps>

## References

- Alexopoulos, A., Dellaportas, P. and Forster, J. J. (2019), 'Bayesian forecasting of mortality rates by using latent Gaussian models', *Journal of the Royal Statistical Society Series A: Statistics in Society* **182**(2), 689–711.
- Antonio, K., Bardoutsos, A. and Ouburg, W. (2015), 'Bayesian Poisson log-bilinear models for mortality projections with multiple populations', *European Actuarial Journal* **5**(2), 245–281.
- Barigou, K., Goffard, P.-O., Loisel, S. and Salhi, Y. (2023), 'Bayesian model averaging for mortality forecasting using leave-future-out validation', *International Journal of Forecasting* **39**(2), 674–690.
- Cairns, A. J., Blake, D., Dowd, K., Coughlan, G. D. and Khalaf-Allah, M. (2011), 'Bayesian stochastic mortality modelling for two populations', *ASTIN Bulletin: The Journal of the IAA* **41**(1), 29–59.
- Cairns, A. J., Blake, D. P., Kessler, A. and Kessler, M. (2020), 'The impact of Covid-19 on future higher-age mortality', *Available at SSRN 3606988*.
- Centers for Disease Control and Prevention (CDC) (1984), 'Heat-related mortality—Latium Region, Italy, summer 1983', *MMWR. Morbidity and mortality weekly report* **33**(37), 518–521.



- Chen, F.-Y., Yang, S. S. and Huang, H.-C. (2022), ‘Modeling pandemic mortality risk and its application to mortality-linked security pricing’, *Insurance: Mathematics and Economics* **106**, 341–363.
- Chen, H. and Cox, S. H. (2009), ‘Modeling mortality with jumps: Applications to mortality securitization’, *Journal of Risk and Insurance* **76**(3), 727–751.
- Conti, S., Meli, P., Minelli, G., Solimini, R., Toccaceli, V., Vichi, M., Beltrano, C. and Perini, L. (2005), ‘Epidemiologic study of mortality during the Summer 2003 heat wave in Italy’, *Environmental Research* **98**(3), 390–399.
- Cox, S. H., Lin, Y. and Wang, S. (2006), ‘Multivariate exponential tilting and pricing implications for mortality securitization’, *Journal of Risk and Insurance* **73**(4), 719–736.
- Czado, C., Delwarde, A. and Denuit, M. (2005), ‘Bayesian Poisson log-bilinear mortality projections’, *Insurance: Mathematics and Economics* **36**(3), 260–284.
- de Valpine, P., Paciorek, C., Turek, D., Michaud, N., Anderson-Bergman, C., Obermeyer, F., Wehrhahn Cortes, C., Rodríguez, A., Temple Lang, D., Paganin, S. and Hug, J. (2023), *NIMBLE: MCMC, Particle Filtering, and Programmable Hierarchical Modeling*. R package version 1.0.1.  
**URL:** <https://cran.r-project.org/package=nimble>
- de Valpine, P., Turek, D., Paciorek, C., Anderson-Bergman, C., Temple Lang, D. and Bodik, R. (2017), ‘Programming with models: writing statistical algorithms for general model structures with NIMBLE’, *Journal of Computational and Graphical Statistics* **26**, 403–417.
- de’Donato, F. K., Leone, M., Noce, D., Davoli, M. and Michelozzi, P. (2013), ‘The impact of the February 2012 cold spell on health in Italy using surveillance data’, *PLoS one* **8**(4), e61720.
- Faust, J. S., Du, C., Renton, B., Liang, C., Chen, A. J., Li, S.-X., Lin, Z., Nunez-Smith, M. and Krumholz, H. M. (2022), ‘Two years of Covid-19: Excess mortality by age, region, gender, and race/ethnicity in the United States during the Covid-19 pandemic, March 1, 2020, through February 28, 2022’, *medRxiv* pp. 2022–08.
- Ferguson, N. M., Laydon, D., Nedjati-Gilani, G., Imai, N., Ainslie, K., Baguelin, M., Bhatia, S., Boonyasiri, A., Cucunubá, Z., Cuomo-Dannenburg, G. et al. (2020), ‘Impact of non-pharmaceutical interventions (npis) to reduce COVID-19 mortality and healthcare demand’, *Imperial College London* (16-03-2020).
- Gagnon, A., Miller, M. S., Hallman, S. A., Bourbeau, R., Herring, D. A., Earn, D. J. and Madrenas, J. (2013), ‘Age-specific mortality during the 1918 influenza pandemic: unravelling the mystery of high young adult mortality’, *PLoS one* **8**(8), e69586.
- Haberman, S. and Renshaw, A. (2012), ‘Parametric mortality improvement rate modelling and projecting’, *Insurance: Mathematics and Economics* **50**(3), 309–333.
- Hunt, A. and Blake, D. (2020), ‘Identifiability in age/period mortality models’, *Annals of Actuarial Science* **14**(2), 461–499.
- Hunt, A. and Villegas, A. M. (2023), ‘Mortality Improvement Rates: Modeling, Parameter Uncertainty, and Robustness’, *North American Actuarial Journal* **27**(1), 47–73.
- Lee, R. D. and Carter, L. R. (1992), ‘Modeling and forecasting US mortality’, *Journal of the American Statistical Association* **87**(419), 659–671.

- Li, J. S.-H., Zhou, K. Q., Zhu, X., Chan, W.-S. and Chan, F. W.-H. (2019), ‘A Bayesian approach to developing a stochastic mortality model for China’, *Journal of the Royal Statistical Society Series A: Statistics in Society* **182**(4), 1523–1560.
- Li, N. and Lee, R. (2005), ‘Coherent mortality forecasts for a group of populations: An extension of the lee-carter method’, *Demography* **42**, 575–594.
- Liu, Y. and Li, J. S.-H. (2015), ‘The age pattern of transitory mortality jumps and its impact on the pricing of catastrophic mortality bonds’, *Insurance: Mathematics and Economics* **64**, 135–150.
- Mitchell, D., Brockett, P., Mendoza-Arriaga, R. and Muthuraman, K. (2013), ‘Modeling and forecasting mortality rates’, *Insurance: Mathematics and Economics* **52**(2), 275–285.
- Monod, M., Blenkinsop, A., Xi, X., Hebert, D., Bershan, S., Tietze, S., Baguelin, M., Bradley, V. C., Chen, Y., Coupland, H. et al. (2021), ‘Age groups that sustain resurging COVID-19 epidemics in the United States’, *Science* **371**(6536), eabe8372.
- Ng, K. W., Tian, G.-L. and Tang, M.-L. (2011), *Dirichlet and Related Distributions: Theory, Methods and Applications*, Wiley, Hoboken, N.J.
- O’Driscoll, M., Ribeiro Dos Santos, G., Wang, L., Cummings, D. A., Azman, A. S., Paireau, J., Fontanet, A., Cauchemez, S. and Salje, H. (2021), ‘Age-specific mortality and immunity patterns of SARS-CoV-2’, *Nature* **590**(7844), 140–145.
- Pedroza, C. (2006), ‘A Bayesian forecasting model: predicting US male mortality’, *Biostatistics* **7**(4), 530–550.
- Pitacco, E. (2009), *Modelling longevity dynamics for pensions and annuity business*, Oxford University Press.
- Richards, S. J. (2023), ‘Robust mortality forecasting in the presence of outliers’, *Preprint* .
- Robben, J. and Antonio, K. (2023), ‘Catastrophe risk in a stochastic multi-population mortality model’, *arXiv preprint arXiv:2306.15271* .
- Rosano, A., Bella, A., Gesualdo, F., Acampora, A., Pezzotti, P., Marchetti, S., Ricciardi, W. and Rizzo, C. (2019), ‘Investigating the impact of influenza on excess mortality in all ages in Italy during recent seasons (2013/14–2016/17 seasons)’, *International Journal of Infectious Diseases* **88**, 127–134.
- Schnürch, S., Kleinow, T., Korn, R. and Wagner, A. (2022), ‘The impact of mortality shocks on modelling and insurance valuation as exemplified by COVID-19’, *Annals of Actuarial Science* **16**(3), 498–526.
- Stan Development Team (2023), ‘RStan: the R interface to Stan’. R package version 2.26.16.  
**URL:** <https://mc-stan.org/>
- Tibbits, M. M., Groendyke, C., Haran, M. and Liechty, J. C. (2014), ‘Automated Factor Slice Sampling’, *Journal of Computational and Graphical Statistics* **23**(2), 543–563.
- van Berkum, F., Melenberg, B. and Vellekoop, M. (2022), ‘Estimating the impact of the COVID-19 pandemic using granular mortality data’, *arXiv preprint arXiv:2209.06473* .
- Vehtari, A., Gabry, J., Magnusson, M., Yao, Y., Bürkner, P.-C., Paananen, T., Gelman, A., Goodrich, B., Piironen, J., Nicenboim, B. and Lindgren, L. (2023), ‘loo: Efficient Leave-One-Out Cross-Validation and WAIC for Bayesian Models’. R package version 2.6.0.

- Vehtari, A., Gelman, A. and Gabry, J. (2017), ‘Practical Bayesian model evaluation using leave-one-out cross-validation and WAIC’, *Statistics and Computing* **27**(5), 1413–1432.
- Vehtari, A., Gelman, A., Simpson, D., Carpenter, B. and Bürkner, P.-C. (2021), ‘Rank-normalization, folding, and localization: An improved  $\widehat{R}$  for assessing convergence of MCMC (with discussion)’, *Bayesian Analysis* **16**(2), 667–718.
- Venter, G. and Şahin, Ş. (2018), ‘Parsimonious parameterization of age-period-cohort models by Bayesian shrinkage’, *ASTIN Bulletin: The Journal of the IAA* **48**(1), 89–110.
- Villegas, A. M., Kaishev, V. K. and Millossovich, P. (2018), ‘StMoMo: An R package for stochastic mortality modeling’, *Journal of Statistical Software* **84**(3), 1–38.
- Watanabe, S. (2010), ‘Asymptotic equivalence of Bayes cross validation and widely applicable information criterion in singular learning theory’, *J. Mach. Learn. Res.* **11**, 3571–3594.
- Wong, J. S., Forster, J. J. and Smith, P. W. (2018), ‘Bayesian mortality forecasting with overdispersion’, *Insurance: Mathematics and Economics* **83**, 206–221.
- Wong, J. S., Forster, J. J. and Smith, P. W. (2023), ‘Bayesian model comparison for mortality forecasting’, *Journal of the Royal Statistical Society Series C: Applied Statistics* **72**(3), 566–586.
- Zhou, R. and Li, J. S.-H. (2022), ‘A multi-parameter-level model for simulating future mortality scenarios with COVID-alike effects’, *Annals of Actuarial Science* **16**(3), 453–477.

## 9 Appendix

### 9.1 Proof of Identification

Identifiability of  $\sigma_r^2$  is obvious. The conditions  $\Delta J_2 = 0$ ,  $\xi_2 = 0$  and  $\sum_x \beta_x = 1$  yield  $\sum_x \mathbb{E}(Z_{x,1}) = d$ , i.e. identifiability of the drift, which in turn implies that  $\Delta \kappa_2 = d$ . Starting from (3.6) with  $\mathbf{B}_x = (\beta_x, \beta_x^{(J)})^\top$  and  $\mathbf{K}_t = (\Delta \kappa_{t+1}, \Delta J_{t+1})^\top$  we can verify identifiability of  $(\beta_x)_x$ ,  $(\beta_x^{(J)})_x$ ,  $(\Delta \kappa_t)_t$  and  $(\Delta J_t)_t$  showing that the only possible choice for the matrix  $\mathbf{A}$  is the identity matrix if the constraints

$$\sum_{x=1}^A \beta_x = \sum_{x=1}^A \tilde{\beta}_x = 1, \quad \sum_{x=1}^A \beta_x^{(J)} = \sum_{x=1}^A \tilde{\beta}_x^{(J)} = 1, \quad \Delta J_1 = \Delta \tilde{J}_1 = 0, \quad \Delta \kappa_1 = \Delta \tilde{\kappa}_1 = d. \quad (9.1)$$

are met. Then, from

$$\begin{pmatrix} d \\ 0 \end{pmatrix} = \tilde{\mathbf{K}}_1 = \begin{pmatrix} a_1 & a_3 \\ a_2 & a_4 \end{pmatrix} \mathbf{K}_1 = \begin{pmatrix} a_1 & a_3 \\ a_2 & a_4 \end{pmatrix} \begin{pmatrix} d \\ 0 \end{pmatrix}$$

we get  $a_1 = 1$  and  $a_2 = 0$  in view of our assumption  $d \neq 0$ . Similarly,

$$\begin{pmatrix} 1 \\ 1 \end{pmatrix} = \sum_x \tilde{\mathbf{B}}_x = \frac{1}{a_1 a_4 - a_2 a_3} \begin{pmatrix} a_4 & -a_3 \\ -a_2 & a_1 \end{pmatrix} \sum_x \mathbf{B}_x = \frac{1}{a_1 a_4 - a_2 a_3} \begin{pmatrix} a_4 & -a_3 \\ -a_2 & a_1 \end{pmatrix} \begin{pmatrix} 1 \\ 1 \end{pmatrix}$$

yields

$$a_4 - a_3 = a_1 - a_2 = a_1 a_4 - a_2 a_3.$$

Hence, we end up with  $a_3 = 0$  and  $a_4 = 1$ . In other words, we achieved identifiability of the parameters of the mortality improvements.

If we assume additionally that  $N_T = J_1 = J_2 = 0$  and that  $(Y_t)_t$  is a sequence of positive parameters, we can even identify the times of jump occurrences  $(N_t)_t$  and the autoregressive parameter  $a$ . To this end, first notice that one obtains  $(J_t)_t$  iteratively from  $J_1 = J_2 = 0$  and knowledge of  $(\Delta J_t)_t$ . Note that if there is no jump, then the parameter  $a$  cannot be identified and can be neglected in the model. Otherwise we can proceed iteratively: Let  $t^*$  denote the time of the first jump event, then we have  $N_t = 0$ ,  $t < t^*$ ,  $N_{t^*} = 1$  and  $Y_{t^*} = J_{t^*}$ . Noting that a jump event at time  $t^*$  implies that  $J_t > 0$  for all  $t \geq t^*$  if  $a > 0$ , we can deduce  $a = 0$  for  $J_t = 0$  for some  $t > t^*$ . In the opposite case, we have  $J_T = a J_{T-1}$  as  $N_T = 0$  by assumption. Hence, we can identify  $a$  and subsequently  $(N_t)_t$  and the  $Y_t$ 's belonging to non-vanishing  $N_t$ 's.

As a final remark, let us mention that instead of assuming  $N_T = 0$  we could also assume that we know a time point  $\tilde{t} > t^*$ , where no jump occurs. Then the whole argument above can be adapted using  $\tilde{t}$  instead of  $T$ . Moreover, instead of assuming positivity of  $(Y_t)_t$  one can alternatively assume that  $J_{T-1} \neq 0$ .

### 9.2 Deriving Dirichlet distributions from Gamma distributions

Let  $X_i$  be a random variable from the Gamma distribution with  $X_i \sim \text{Gamma}(\alpha_i, 1)$ , where  $i = 1, \dots, k$ . Further, let

$$Y_i = \frac{X_i}{X_1 + X_2 + \dots + X_k}. \quad (9.2)$$

Then, the joint density of  $Y_1, \dots, Y_{k-1}$  is

$$f(y_1, \dots, y_{k-1}) = \frac{\alpha_1 + \dots + \alpha_k}{\Gamma(\alpha_1) \dots \Gamma(\alpha_k)} y_1^{\alpha_1-1} \dots y_{k-1}^{\alpha_{k-1}-1} (1 - y_1 - \dots - y_{k-1})^{\alpha_k-1}, \quad (9.3)$$

where  $y_i > 0, i = 1, \dots, k-1, y_1 + \dots + y_{k-1} < 1$ . The above joint pdf of  $Y_1, \dots, Y_{k-1}$  happens to be the pdf of a Dirichlet distribution with parameters  $\alpha_1, \dots, \alpha_k$  for the random vector  $(Y_1, \dots, Y_k)$ , with  $y_k = 1 - y_1 - \dots - y_{k-1}$ . For proof see e.g. [Ng et al. \(2011\)](#).

Hence, instead of sampling  $\beta$  from a Dirichlet distribution, we can also sample Gamma distributed random variables  $b_1, \dots, b_A$  and apply the transformation of (9.2) by setting

$$\beta_x = \frac{b_x}{b_1 + \dots + b_A}, \text{ for all } x \in \{1, \dots, A-1\}$$

and  $\beta_A = (1 - \beta_1 - \dots - \beta_{A-1})$ . This allows us to use a wider variety of samplers, like the multivariate slice sampler of [Tibbits et al. \(2014\)](#), improving convergence.

### 9.3 Tables of parameter estimates

#### 9.3.1 England and Wales

Table 4: Posterior estimates for England and Wales data using our model.

Parameter	Mean	MAP	Sd	10%-PI	90PI	split- $\hat{R}$	Tail_ESS	Bulk_ESS
$\beta_1$	0.11	0.11	0.01	0.10	0.12	1.00	1903	1858
$\beta_2$	0.26	0.26	0.01	0.25	0.27	1.00	1968	1849
$\beta_3$	0.15	0.15	0.01	0.14	0.16	1.00	2056	1964
$\beta_4$	0.07	0.07	0.01	0.05	0.08	1.00	1686	2048
$\beta_5$	0.07	0.07	0.01	0.06	0.08	1.00	1927	1728
$\beta_6$	0.09	0.09	0.01	0.08	0.10	1.00	2011	1830
$\beta_7$	0.08	0.08	0.01	0.07	0.09	1.00	2053	1887
$\beta_8$	0.06	0.06	0.01	0.05	0.07	1.00	2029	1877
$\beta_9$	0.06	0.06	0.01	0.05	0.07	1.00	2012	1802
$\beta_{10}$	0.06	0.05	0.01	0.05	0.07	1.00	1876	1699
$\beta_1^{(J)}$	0.01	0.00	0.00	0.00	0.01	1.00	928	1019
$\beta_2^{(J)}$	0.08	0.08	0.01	0.07	0.09	1.00	375	746
$\beta_3^{(J)}$	0.08	0.08	0.01	0.07	0.09	1.00	863	1638
$\beta_4^{(J)}$	0.37	0.37	0.01	0.35	0.38	1.00	352	385
$\beta_5^{(J)}$	0.29	0.29	0.01	0.28	0.31	1.01	298	419
$\beta_6^{(J)}$	0.11	0.11	0.01	0.10	0.12	1.00	1840	1854
$\beta_7^{(J)}$	0.03	0.04	0.01	0.03	0.04	1.00	1393	1708
$\beta_8^{(J)}$	0.01	0.01	0.01	0.01	0.02	1.00	1021	1249
$\beta_9^{(J)}$	0.01	0.01	0.01	0.00	0.02	1.00	1594	1898
$\beta_{10}^{(J)}$	0.00	0.00	0.00	0.00	0.01	1.00	1712	1719
$d$	-0.21	-0.21	0.04	-0.26	-0.15	1.00	1946	1981
$\sigma_\xi$	0.47	0.46	0.04	0.42	0.52	1.00	2034	1964
$\sigma_r$	0.04	0.04	0.00	0.04	0.05	1.00	1840	1783
$p$	0.10	0.10	0.03	0.07	0.13	1.00	1939	2004
$a$	0.24	0.23	0.05	0.20	0.26	1.01	390	156
$\mu_Y$	2.21	2.31	0.52	1.58	2.86	1.00	596	298
$\sigma_Y$	1.66	1.58	0.37	1.24	2.15	1.00	528	883

### 9.3.2 United States

Table 5: Posterior estimates for the United States data using our model.

Parameter	Mean	MAP	Sd	10%-PI	90%-PI	split- $\hat{R}$	Bulk-ESS	Tail-ESS
$\beta_1$	0.13	0.13	0.02	0.10	0.15	1.00	2021	1815
$\beta_2$	0.17	0.16	0.02	0.14	0.20	1.00	1983	1797
$\beta_3$	0.15	0.15	0.02	0.12	0.18	1.00	1945	1886
$\beta_4$	0.18	0.17	0.02	0.15	0.20	1.00	2101	1894
$\beta_5$	0.15	0.15	0.02	0.12	0.17	1.00	2014	1931
$\beta_6$	0.07	0.07	0.02	0.05	0.10	1.00	2049	1976
$\beta_7$	0.06	0.07	0.02	0.04	0.09	1.00	1481	1847
$\beta_8$	0.05	0.05	0.02	0.03	0.08	1.00	1859	1800
$\beta_9$	0.03	0.02	0.02	0.01	0.05	1.00	1971	1927
$\beta_{10}$	0.01	0.00	0.01	0.00	0.03	1.00	1937	1885
$\beta_1^{(J)}$	0.01	0.00	0.01	0.00	0.01	1.00	1827	1987
$\beta_2^{(J)}$	0.02	0.02	0.01	0.00	0.04	1.00	1364	1839
$\beta_3^{(J)}$	0.13	0.14	0.01	0.12	0.15	1.00	2052	1826
$\beta_4^{(J)}$	0.16	0.15	0.01	0.14	0.17	1.00	1719	1925
$\beta_5^{(J)}$	0.16	0.16	0.01	0.14	0.17	1.00	2055	1925
$\beta_6^{(J)}$	0.14	0.14	0.01	0.12	0.16	1.00	1889	2005
$\beta_7^{(J)}$	0.11	0.11	0.01	0.10	0.13	1.00	2038	1927
$\beta_8^{(J)}$	0.10	0.10	0.01	0.08	0.11	1.00	1805	1859
$\beta_9^{(J)}$	0.09	0.09	0.01	0.08	0.11	1.00	1948	1835
$\beta_{10}^{(J)}$	0.08	0.08	0.01	0.07	0.10	1.00	2046	1982
$d$	-0.11	-0.10	0.03	-0.15	-0.07	1.00	1938	1946
$\sigma_\xi$	0.19	0.18	0.03	0.16	0.23	1.00	1797	1865
$\sigma_r$	0.02	0.02	0.00	0.02	0.02	1.00	1861	1867
$p$	0.05	0.04	0.03	0.02	0.09	1.00	1984	1874
$a$	0.46	0.47	0.07	0.37	0.55	1.00	1735	1799
$\mu_Y$	1.37	1.34	0.59	0.68	2.00	1.00	1207	902
$\sigma_Y$	0.85	0.29	0.72	0.20	1.77	1.00	238	401

### 9.3.3 Spain

Table 6: Posterior estimates for Spain data using our model.

Parameter	Mean	MAP	Sd	10%-PI	90%-PI	Split- $\hat{R}$	Bulk-ESS	Tail-ESS
$\beta_1$	0.13	0.13	0.02	0.11	0.16	1.00	1799	1661
$\beta_2$	0.16	0.16	0.02	0.14	0.18	1.00	2033	1931
$\beta_3$	0.18	0.18	0.02	0.16	0.21	1.00	1936	1926
$\beta_4$	0.16	0.16	0.02	0.14	0.19	1.00	2120	1969
$\beta_5$	0.10	0.11	0.02	0.08	0.13	1.00	1915	1779
$\beta_6$	0.03	0.04	0.02	0.01	0.06	1.00	2029	2049
$\beta_7$	0.04	0.04	0.02	0.02	0.06	1.00	1718	1826
$\beta_8$	0.06	0.06	0.02	0.04	0.08	1.00	2010	1942
$\beta_9$	0.07	0.07	0.02	0.04	0.09	1.00	1962	1810
$\beta_{10}$	0.06	0.06	0.02	0.04	0.08	1.00	1931	1788
$\beta_1^{(J)}$	0.02	0.01	0.02	0.00	0.05	1.00	1888	1838
$\beta_2^{(J)}$	0.01	0.00	0.01	0.00	0.02	1.00	1995	1962
$\beta_3^{(J)}$	0.06	0.07	0.03	0.02	0.10	1.00	1765	1964
$\beta_4^{(J)}$	0.16	0.16	0.03	0.12	0.19	1.00	1748	1849
$\beta_5^{(J)}$	0.12	0.12	0.03	0.08	0.15	1.00	2153	1888
$\beta_6^{(J)}$	0.06	0.06	0.02	0.03	0.10	1.00	2133	2008
$\beta_7^{(J)}$	0.08	0.08	0.03	0.05	0.12	1.00	1937	1937
$\beta_8^{(J)}$	0.13	0.12	0.03	0.09	0.16	1.00	1941	1806
$\beta_9^{(J)}$	0.19	0.18	0.03	0.15	0.22	1.00	1663	1925
$\beta_{10}^{(J)}$	0.17	0.17	0.03	0.13	0.21	1.00	1720	1918
$d$	-0.24	-0.24	0.05	-0.30	-0.18	1.00	1846	2050
$\sigma_\xi$	0.31	0.30	0.04	0.26	0.37	1.00	1957	1938
$\sigma_r$	0.04	0.04	0.00	0.03	0.04	1.00	1764	1926
$p$	0.04	0.02	0.03	0.01	0.08	1.00	933	984
$a$	0.22	0.18	0.11	0.08	0.36	1.00	1839	1763
$\mu_Y$	1.05	0.86	0.68	0.29	1.96	1.01	279	588
$\sigma_Y$	0.93	0.55	0.53	0.32	1.70	1.01	179	179



### 9.3.4 Italy

Table 7: Posterior estimates for Italian data using our model.

Parameter	Mean	MAP	Sd	10%-PI	90%-PI	split- $\hat{R}$	Bulk-ESS	Tail-ESS
$\beta_1$	0.15	0.15	0.02	0.12	0.18	1.00	2013	1967
$\beta_2$	0.21	0.21	0.02	0.17	0.24	1.00	1782	1635
$\beta_3$	0.15	0.15	0.02	0.12	0.18	1.00	2181	1926
$\beta_4$	0.13	0.13	0.02	0.11	0.16	1.00	2081	2049
$\beta_5$	0.08	0.08	0.02	0.05	0.10	1.00	1871	1876
$\beta_6$	0.07	0.07	0.02	0.05	0.10	1.00	1754	1882
$\beta_7$	0.06	0.06	0.02	0.04	0.09	1.00	2019	1895
$\beta_8$	0.06	0.06	0.02	0.04	0.09	1.00	1940	1876
$\beta_9$	0.06	0.06	0.02	0.03	0.08	1.00	2038	2057
$\beta_{10}$	0.03	0.03	0.02	0.01	0.05	1.00	1779	1696
$\beta_1^{(J)}$	0.05	0.04	0.03	0.01	0.09	1.00	1938	1809
$\beta_2^{(J)}$	0.03	0.01	0.02	0.00	0.06	1.00	1630	1925
$\beta_3^{(J)}$	0.02	0.01	0.02	0.00	0.05	1.00	1805	1837
$\beta_4^{(J)}$	0.02	0.00	0.02	0.00	0.05	1.00	1938	2007
$\beta_5^{(J)}$	0.04	0.05	0.03	0.01	0.08	1.00	1874	1861
$\beta_6^{(J)}$	0.10	0.10	0.03	0.06	0.15	1.00	1877	1924
$\beta_7^{(J)}$	0.13	0.13	0.03	0.09	0.17	1.00	2020	1966
$\beta_8^{(J)}$	0.17	0.17	0.03	0.13	0.21	1.00	1914	2008
$\beta_9^{(J)}$	0.21	0.21	0.03	0.17	0.26	1.00	1894	1887
$\beta_{10}^{(J)}$	0.22	0.21	0.04	0.18	0.27	1.00	1629	1614
$d$	-0.20	-0.20	0.04	-0.25	-0.15	1.00	1741	1933
$\sigma_\xi$	0.23	0.21	0.03	0.19	0.27	1.00	1296	1682
$\sigma_r$	0.04	0.04	0.00	0.04	0.04	1.00	1938	1758
$p$	0.12	0.10	0.05	0.06	0.20	1.00	1304	1646
$a$	0.16	0.03	0.12	0.02	0.34	1.00	1630	1961
$\mu_Y$	0.32	0.30	0.13	0.17	0.47	1.00	647	800
$\sigma_Y$	0.24	0.17	0.15	0.10	0.41	1.01	268	367

## 9.4 Prior parameterisation by country

Table 8: Prior parameterisation for the England and Wales Data.

Parameter	Prior Distribution	Hyperprior 1	Hyperprior 2
<b>Age Parameter</b>			
$(\beta_1, \dots, \beta_A)$	Dirichlet(1, ..., 1)	-	-
$(\beta_1^{(J)}, \dots, \beta_A^{(J)})$	Dirichlet(1, 1, 1, 5, 5, 5, 5, 1, 1, 1)	-	-
<b>Time Parameter</b>			
$\Delta\kappa_t$	$\Delta\kappa_t \stackrel{iid}{\sim} \mathcal{N}(d, \sigma_\xi^2)$	$d \sim \mathcal{N}(0, 5^2)$	$\sigma_\xi \sim \mathcal{N}_+(0, 2^2)$
$N_t$	$N_t \stackrel{iid}{\sim} \text{Bern}(p)$	$p \sim \text{Beta}(1, 20)$	-
$Y_t$	$Y_t \stackrel{iid}{\sim} \mathcal{N}(\mu_Y, \sigma_Y^2)$	$\mu_Y \sim \mathcal{N}_+(1, 2^2)$	$\sigma_Y \sim \mathcal{N}_+(0, 2^2)$
$a$	$a \sim \text{Beta}(1, 5)$	-	-
<b>Other Parameters</b>			
$\sigma_\varepsilon$	$\sigma_\varepsilon \sim \mathcal{N}_+(0, 2^2)$	-	-

Table 9: Prior parameterisation for all countries using COVID data (US, Spain and Italy).

Parameter	Prior Distribution	Hyperprior 1	Hyperprior 2
<b>Age Parameter</b>			
$(\beta_1, \dots, \beta_A)$	Dirichlet(1, ..., 1)	-	-
$(\beta_1^{(J)}, \dots, \beta_A^{(J)})$	Dirichlet(1, ..., 1)	-	-
<b>Time Parameter</b>			
$\Delta\kappa_t$	$\Delta\kappa_t \stackrel{iid}{\sim} \mathcal{N}(d, \sigma_\xi^2)$	$d \sim \mathcal{N}(0, 2^2)$	$\sigma_\xi \sim \mathcal{N}_+(0, 2^2)$
$N_t$	$N_t \stackrel{iid}{\sim} \text{Bern}(p)$	$p \sim \text{Beta}(1, 20)$	-
$Y_t$	$Y_t \stackrel{iid}{\sim} \mathcal{N}(\mu_Y, \sigma_Y^2)$	$\mu_Y \sim \mathcal{N}_+(0, 4^2)$	$\sigma_Y \sim \mathcal{N}_+(0, 2^2)$
$a$	$a \sim \text{Beta}(1, 5)$	-	-
<b>Other Parameters</b>			
$\sigma_r$	$\sigma_r \sim \mathcal{N}_+(0, 2^2)$	-	-

## 9.5 Overview of used samplers for our model

Table 10: Overview of selected samplers for our model.

Sampler	Parameter
AF Slice Sampler	$(\beta_1, \dots, \beta_A)$ $(\beta_1^{(J)}, \dots, \beta_A^{(J)})$
Binary Sampler	$N_t \quad \forall t \in \{1, \dots, T-1\}$
Gibbs	$d$ $p$ $\Delta\kappa_t \quad \forall t \in \{1, \dots, T\}$
Random Walk Metropolis	$\sigma_r$ $\sigma_\xi$
Slice Sampler	$Y_t \quad \forall t \in \{1, \dots, T\}$ $\mu_Y$ $\sigma_Y$ $a$